Article

The Origin of Magnetic Anisotropy and Single-Molecule Magnet Behavior in Chromium(II)-Based Extended Metal Atom Chains

Andrea Cornia,* Anne-Laure Barra, Vladimir Bulicanu, Rodolphe Clérac, Miguel Cortijo, Elizabeth A. Hillard,* Rita Galavotti, Alessandro Lunghi, Alessio Nicolini, Mathieu Rouzières, Lorenzo Sorace, and Federico Totti*
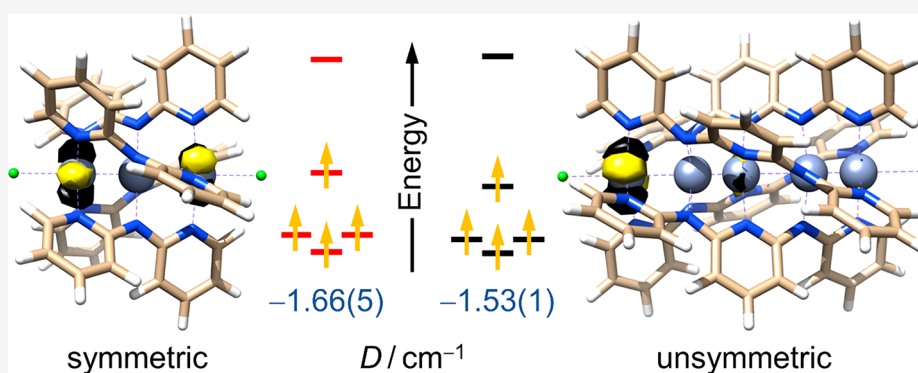
Read Online

ACCESS | 📊 Metrics & More | 📄 Article Recommendations | 🆂🅸 Supporting Information

ABSTRACT: Chromium(II)-based extended metal atom chains have been the focus of considerable discussion regarding their symmetric versus unsymmetric structure and magnetism. We have now investigated four complexes of this class, namely, $[Cr_3(dpa)_4X_2]$ and $[Cr_5(tpda)_4X_2]$ with X = Cl^- and SCN^- [Hdpa = dipyridin-2-yl-amine; $H_2tpda = N^2,N^6$-di(pyridin-2-yl)pyridine-2,6-diamine]. By dc/ac magnetic techniques and EPR spectroscopy, we found that all these complexes have easy-axis anisotropies of comparable magnitude in their S = 2 ground state ($|D| = 1.5−1.8$ cm^{-1}) and behave as single-molecule magnets at low T. Ligand-field and DFT/CASSCF calculations were used to explain the similar magnetic properties of tri- versus pentachromium(II) strings, in spite of their different geometrical preferences and electronic structure. For both X ligands, the ground structure is unsymmetric in the pentachromium(II) species (i.e., with an alternation of long and short Cr−Cr distances) but is symmetric in their shorter congeners. Analysis of the electronic structure using quasi-restricted molecular orbitals (QROs) showed that the four unpaired electrons in Cr$_5$ species are largely localized in four 3d-like QROs centered on the terminal, "isolated" Cr^{2+} ion. In Cr$_3$ complexes, they occupy four nonbonding combinations of 3d-like orbitals centered only on the two terminal metals. In both cases, then, QRO eigenvalues closely mirror the 3d-level pattern of the terminal ions, whose coordination environment remains quite similar irrespective of chain length. We conclude that the extent of unpaired-electron delocalization has little impact on the magnetic anisotropy of these wire-like molecular species.

INTRODUCTION

Single-molecule magnets (SMMs) are molecules comprising one or more metal centers and showing slow relaxation of the magnetization below a characteristic temperature, referred to as the blocking temperature (T_B).[1,2] They are considered as the smallest chemically tunable components for spin-based devices and hold promise for applications in information storage[3−5] and quantum technologies.[6−9] A key ingredient for SMM behavior is magnetic anisotropy, which mainly originates from spin−orbit coupling and crystal-field effects.[10,11] Although cases of slow magnetic relaxation are known for predominantly easy-plane systems,[12,13] the vast majority of known SMMs have an easy-axis anisotropy in their ground state. The reversal of the magnetic moment is then subject to

an energy barrier, U, whose height is one of the important factors that rule magnetic relaxation.[14,15] A recent breakthrough in the field was the discovery that remarkably large energy barriers can be achieved even in mononuclear species.[13,16] Lanthanoid complexes of this type are indeed among the best SMMs known to date,[17−24] with U/k_B values above 2000 K and record observable T_B values of up to 80 K.[22−24]

Examples of SMMs have been recently reported in polynuclear compounds containing metal−metal bonds and exhibiting, as a unique feature, a well-isolated high-spin ground state even at room temperature. The current record spin value is $S = 11$ for a mixed-valent hexairon complex with an octahedral metal topology.[25] Similar features are encountered in the so-called extended metal atom chains (EMACs), which have attracted attention as molecular analogues of macroscopic wires and benchmark systems for understanding metal−metal interactions.[26−29] EMACs consist of three or more metal centers forming a linear array supported by three or four deprotonated oligo-α-pyridylamine (or related) ligands, most often arranged in a helical fashion.[30−32] Their molecular wire-like structure has either rigorous or idealized axial symmetry and makes high-spin EMACs potential SMMs. In fact, the tri- and pentachromium(II) compounds $[Cr_3(dpa)_4Cl_2] \cdot CH_2Cl_2$ ($1a \cdot CH_2Cl_2$)[33] and $[Cr_5(tpda)_4Cl_2] \cdot 4CHCl_3 \cdot 2Et_2O$ ($2a \cdot 4CHCl_3 \cdot 2Et_2O$)[34] have a well-isolated $S = 2$ state, display an easy-axis anisotropy of similar magnitude, and behave as SMMs with energy barriers of 10.6(6) and 8.6(5) K, respectively [Hdpa = dipyridin-2-yl-amine; H_2tpda = N^2,N^6-di(pyridin-2-yl)pyridine-2,6-diamine; see Scheme 1].[35−37] The similarity in magnetic behavior is surprising since the electronic structure of the two string-like complexes is thought to be different. After considerable initial controversy,[38] there is now a general consensus that the abnormally elongated displace-ment ellipsoids of inner metal ions in the crystal structures of pentachromium(II) species reflect a disordered superposition of two unsymmetric structures with alternating short ($d_<$) and long ($d_>$) Cr−Cr distances (Scheme 1d). Resolution of the disorder afforded $d_< = 1.86−2.07$ Å, $d_> = 2.50−2.66$ Å, and $\Delta d = d_> − d_< \sim 0.5−0.8$ Å in compounds $[Cr_5(tpda)_4X_2] \cdot$solv (X = Cl^-, SCN^-)[38] at 213 K, suggesting the presence of two quadruply bonded Cr_2 units *plus* one terminal Cr^{2+} ion. Density functional theory (DFT) indeed predicts the gas phase unsymmetric structure of **2a** to be more stable than the symmetric one by 2.9 kcal mol^{-1} (Scheme 1b,d; X = Cl^-).[39] As a result, the $S = 2$ state of **2a** is largely localized on one of the terminal five-coordinate high-spin Cr^{2+} ions. Other penta-[40] as well as hepta-[41] and nonachromium(II)[42] strings exhibit similar structural features, sometimes with attenuated Δd values. It should be mentioned that $^1H/^2H$ NMR signals from **2a** in dichloromethane solution reveal a symmetric config-uration, suggesting fast switching between the two unsym-metric forms on the NMR time scale.[39]

Things are different in trichromium(II) EMACs, which exhibit greater structural diversity as a function of both axial and equatorial ligands.[33,43−45] The largest structural study so far available was performed by Cotton and Murillo et al., who used X-ray crystallography to investigate 14 compounds with the formula $[Cr_3(dpa)_4X_2] \cdot$solv (X = BF_4^-, NO_3^-, CH_3CN, Cl^-, Br^-, I^-, SCN^-, OCN^-, CN^-, PhCC$^-$) at the same temperature (213 K).[33,43,44] For all axial ligands, with the exception of the strongest σ donors (X = CN^- and PhCC$^-$), the central Cr^{2+} ion features an abnormally elongated displacement ellipsoid, which was taken as evidence of an orientationally disordered unsymmetric structure (Scheme 1c). Refinement using a split-atom model was then undertaken,[43] which in the vast majority of cases gave Δd values of 0.22−0.32 Å, i.e., distinctly *smaller* than in the pentachromium-(II) complexes. Only with very weak axial ligands (X = BF_4^-, NO_3^-) does the geometrical distortion reach 0.6−0.7 Å, thereby approaching those observed in the higher-membered congeners and in $[Cr_3(dpa)_4XY]$ structures with two different axial groups (X = Cl^-; Y = BF_4^-, PF_6^-).[33]

In 2014, an illuminating temperature-dependent structural study was published by Overgaard and Iversen et al.[46] They showed that at 15 K the structure of $1a \cdot Et_2O$ is symmetric (Scheme 1a) within 0.002 Å and that at this temperature the vibrational amplitude of the central Cr^{2+} ion along the chain axis is only slightly larger than for the terminal ions ($\Delta U < 30 \times 10^{-4}$ Å^2). The difference becomes much larger at 100 K, indicating that the central metal is not positionally disordered but lies in a shallow potential energy surface.[46] It was argued that the $S = 2$ state of **1a** is a delocalized molecular state in the temperature regime where SMM behavior manifests itself.[36] The observed low-temperature structure perfectly matches DFT theoretical predictions published in 2001 by Bénard and Rohmer et al.[47] These authors first showed that **1a** has a quintet ground state in the gas phase, with a symmetric equilibrium structure supported by a 3-center-3-electron σ bond involving the metal $3d_{z^2}$ orbitals. The remaining π and δ orbitals contribute negligibly to the bonding, and distortion of the symmetric structure is an energetically facile process (∼1 and ∼4 kcal mol^{-1} for $\Delta d = 0.106$ and 0.679 Å, respectively). More recent theoretical work on other $[Cr_3(dpa)_4X_2]$ derivatives has depicted a similar scenario,[48−50] with very flat potential energy landscapes and a prominent role of thermal energy and crystal packing on molecular geometry.[51] This

Scheme 1. Hdpa and H₂tpda Ligands and Structure of the $[Cr_3(dpa)_4X_2]$ (a,c) and $[Cr_5(tpda)_4X_2]$ (b,d) Complexes in Their Symmetric (a,b) and Unsymmetric (c,d) Forms
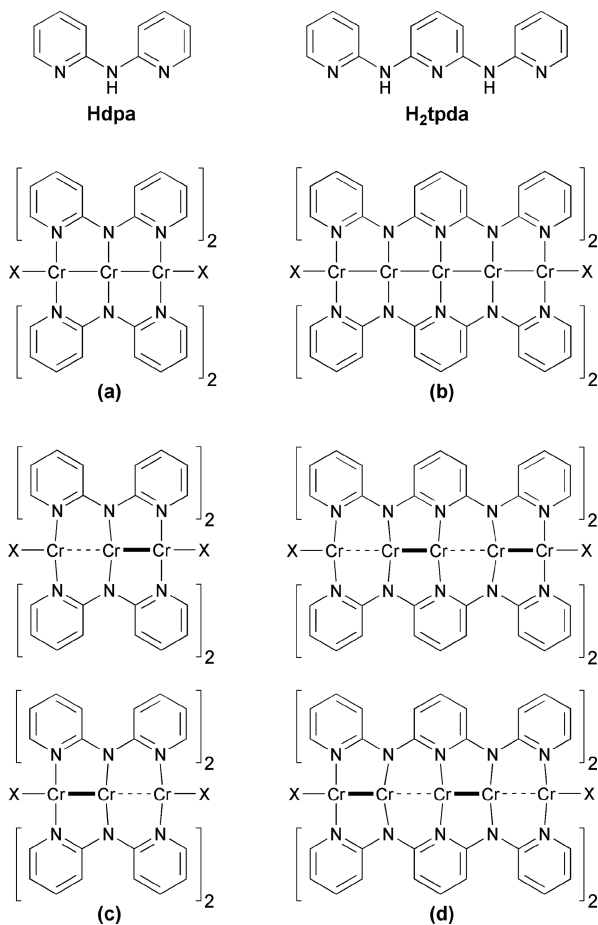
interpretation is also consistent with the fact that solutions of **1a**[52] and $[Cr_3(dpa)_4(N_3)_2]$[53] in dichloromethane show three ^1H NMR resonances, that is, only one less than expected for a symmetric structure over NMR time scale. The *ortho* protons of the dpa$^-$ ligands are most probably paramagnetically shifted and broadened beyond detection, as found in **2a**.[39]

We have now undertaken a wider magnetic and spectroscopic study on odd-membered chromium(II)-based EMACs, focusing on magnetic anisotropy and SMM behavior as a function of chain length and axial ligands. Our investigation covers chlorido derivatives **1a·Et₂O** and **2a·4CHCl₃·2Et₂O**, as well as the isothiocyanato adducts $[Cr_3(dpa)_4(NCS)_2]\cdot$ $0.4CH_2Cl_2$ (**1b·0.4CH₂Cl₂**) and $[Cr_5(tpda)_4(NCS)_2]$ (**2b**). We found that an easy-axis anisotropy and magnetic blocking observed under an applied magnetic field are general properties of these EMACs. With the aid of the angular overlap model (AOM) and DFT/CASSCF calculations, our findings shed new light on an old controversy concerning the amount of spin delocalization in these systems and give an explanation as to why similar magnetic properties arise in tri- and pentachromium(II) species despite their different structural preferences and electronic structure.

■ EXPERIMENTAL SECTION

Materials and Methods. Unless otherwise noted, reagents and solvents were of commercial origin and were used without further purification. Acetonitrile and dichloromethane were purified using an Inert Technologies solvent purification system, while anhydrous *n*-hexane (Sigma-Aldrich) was degassed by bubbling it with Ar before use. All reactions involving chromium(II) complexes were carried out under Ar or N₂ atmosphere using Schlenk techniques or glovebox methods. Compounds **1a·Et₂O**,[33,43,46,52] **2a·4CHCl₃·2Et₂O**,[34] and **2b**[34,41] were prepared by literature procedures or slight modifications thereof (see the Supporting Information and Table S1). Elemental analysis was carried out on a Thermofisher Scientific Flash EA1112 elemental analyzer by the PLACAMAT service (University of Bordeaux, CNRS UMS 3626). The IR spectra were measured on a Nicolet 6700 FT-IR spectrometer using a Smart iTR accessory between 600 and 4000 cm^{-1} with 4 cm^{-1} resolution.

Synthesis of [Cr₃(dpa)₄(NCS)₂]·0.4CH₂Cl₂ (1b·0.4CH₂Cl₂). Preparation was accomplished by a modification of the literature procedure reported by Cotton and Murillo et al.[43] In a glovebox, **1a·Et₂O** (100 mg, 0.102 mmol) and TlBF₄ (64 mg, 0.21 mmol) were dissolved in CH₃CN (15 mL). The mixture was stirred overnight and then filtered through a PTFE filter (0.2 μm porosity, VWR). To this solution, a solution of KSCN (22 mg, 0.23 mmol) in CH₃CN (5 mL) was added, and a dark green precipitate formed immediately. The mixture was filtered, and the precipitate was washed with CH₃CN and dissolved in CH₂Cl₂ (15 mL). The solution was filtered and layered with *n*-hexane in a Schlenk tube. After 1 week, the brownish-green rectangular platelets so-obtained were collected in a glovebox and washed with *n*-hexane (65 mg, 64%). Anal. calcd for $C_{42.4}H_{32.8}Cl_{0.8}Cr_3N_{14}S_2$ (**1b·0.4CH₂Cl₂**, 986.89): C, 51.60; H, 3.35; N, 19.87. Found: C, 51.41; H, 3.45; N, 19.49. IR (ATR): $\tilde{\nu}_{max}$ (cm^{-1}) 2025m (C≡N), 1605m, 1595s, 1547w, 1463s sh, 1456s, 1420s, 1364s br, 1309m, 1277w, 1153s, 1106w, 1052w, 1013m, 917w, 880m, 856w, 800w, 761s, 737m, 644m.

Single-Crystal X-ray Diffraction. A single-crystal X-ray diffraction measurement on **1b·0.4CH₂Cl₂** was carried out using a Bruker Quazar SMART APEXII diffractometer with Mo−Kα radiation. The compound crystallized as brownish-green plates, which had the tendency to stack upon one another. This difficulty, compounded by the large unit cell, made it challenging to obtain a high-quality structure. A small, thin plate suitable for X-ray diffraction was finally selected under immersion oil in ambient conditions and attached to a MiTeGen MicroLoop. The crystal was mounted in a stream of cold N₂ at 120(2) K and centered in the X-ray beam using a

video camera. The data were collected using a routine to survey reciprocal space, and reduction was performed using software included in the Bruker APEX2 suite.[54] The structure was solved using direct methods and refined by least-squares cycles on F^2 followed by difference Fourier syntheses.[55] All hydrogen atoms were included in the final structure factor calculation at idealized positions and were allowed to ride on the neighboring atoms with relative isotropic displacement coefficients. Three independent Cr₃ complexes were found in the asymmetric unit. In all Cr₃ units the electron density associated with the central metal was invariably single peaked and was modeled in two different ways, i.e., as a single Cr atom undergoing anisotropic displacement (Model I or "unsplit-atom" model)[33] or as a Cr atom disordered over two positions; in this case the two components were constrained to have the same isotropic displacement parameter and their occupancies were freely refined but forced to sum up to unity (Model II, or "split-atom" model).[43] As an outcome of Model I, the central metal atoms have significantly larger mean-square displacement amplitudes (U) along the Cr−Cr directions than the terminal metal atoms. ΔU values range from 87 to 164×10^{-4} Å^2 and are hence comparable to those found in **1a·Et₂O** at 100 K ($98–110 \times 10^{-4}$ Å^2).[46] By contrast, the Cr−N(CS) bonds are much more rigid ($\Delta U \leq 30 \times 10^{-4}$ Å^2). Since only in molecule Cr1−Cr2−Cr3 is the displacement ellipsoid of the central metal atom distinctly prolate along the chain axis, Model II was applied to Cr2 only. Crystal and refinement data (Model I) are available as Table S2, whereas selected geometrical parameters are gathered in Tables 1 and S3.

Table 1. Selected Bond Distances (Å) and Angles (deg) in 1b·0.4CH₂Cl₂ Resulting from Model I^a

	molecule A	molecule B	molecule C
$Cr_{T1}−Cr_C$	2.3060(12)	2.3446(13)	2.3527(8)
$Cr_C−Cr_{T2}$	2.3526(11)	2.3565(13)	2.3527(8)
$Cr_{T1}−N_{eq}$	2.115[4]	2.115[4]	2.108[5]
$Cr_C−N_{eq}$	2.026[4]	2.024[5]	2.032[6]
$Cr_{T2}−N_{eq}$	2.109[4]	2.110[5]	2.108[5]
$Cr_{T1}−N_{ax}$	2.200(4)	2.226(5)	2.216(5)
$Cr_{T2}−N_{ax}$	2.208(4)	2.197(5)	2.216(5)
$Cr_{T1}−Cr_C−Cr_{T2}$	179.14(5)	177.73(5)	179.32(8)
$Cr_{T1}−N_{ax}−C$	153.4(4)	147.6(4)	165.1(5)
$Cr_{T2}−N_{ax}−C$	144.2(4)	155.8(5)	165.1(5)
$(Cr_{T1}−)N_{ax}−C−S$	178.7(5)	177.6(6)	179.2(6)
$(Cr_{T2}−)N_{ax}−C−S$	177.6(5)	179.1(6)	179.2(6)

^{a}Cr$_C$ = central Cr^{2+} ion, Cr$_{T1}$ and Cr$_{T2}$ = terminal Cr^{2+} ions, N$_{eq}$ = equatorial nitrogen donor from dpa$^-$, N$_{ax}$ = axial nitrogen donor from isothiocyanate.

Magnetic Measurements. The magnetic measurements were obtained with a Quantum Design MPMS-XL SQUID magnetometer and a PPMS-9 susceptometer. The MPMS-XL instrument works between 1.8 and 400 K with applied direct current (dc) fields (H) ranging from −70 to 70 kOe. The alternating current (ac) susceptibility measurements were performed using an oscillating field of 3−5 Oe for frequencies from 1 to 1500 Hz (MPMS-XL) and an oscillating field of 1−6 Oe for frequencies from 10 Hz to 10 kHz (PPMS-9). Details on sample preparation are given in the Supporting Information. All magnetic data were corrected for the sample holder and for addenda (when used) and were reduced using the appropriate molar mass and a correction for diamagnetism.[56] The dc magnetic susceptibility (χ) was obtained as M/H from magnetization (M) measurements at 1 and 10 kOe in the temperature ranges of 1.85− 295 K (**1a·Et₂O**), 1.85−300 K (**1b·0.4CH₂Cl₂** and **2b**), 1.85−320 K (**2a**), and 1.86−255 K (**2a·4CHCl₃·2Et₂O**). Isothermal magnetization data were also recorded between 1.8 and 10 K in fields up to 70 kOe for all samples. Above 1.8 K, no hysteresis effects were observed in the field dependence of the magnetization for field sweep rates between about 70 and 600 Oe min^{-1}. The ac susceptibility data were measured

down to 1.8 K at frequencies up to 10 kHz, with applied dc fields of zero to 10 kOe. In the available temperature and frequency ranges, all samples displayed slow relaxation of the magnetization only observable in an applied dc field. The optimal dc field value was determined by variable-field ac studies at the lowest reachable temperature. All ac measurements were fitted to the generalized Debye model (using χ' and χ'' vs ν data)[57,58] in order to extract the characteristic relaxation time (τ), the α parameter describing the width of the distribution of relaxation times, as well as the values of χ_0 and χ_∞. The α values at the lowest temperatures were ∼0.07 (**1a**· Et$_2$O), ∼0.3 (**1b**·0.4CH$_2$Cl$_2$), and ∼0.2 (**2a**, **2a**·4CHCl$_3$·2Et$_2$O, and **2b**) and decreased to ∼0 upon heating. Detailed results of dc and ac magnetic characterization are presented in Figures S1−S30 and Table S4.

EPR Spectroscopy. W-band ($\nu \sim 94$ GHz) EPR spectra were recorded using a Bruker Elexsys E600 spectrometer, equipped with a continuous ^{4}He flow CF935 Cryostat (Oxford Instruments). Microcrystalline powder samples were prepared by crushing single crystals of the different compounds in a glovebox. The sample was mixed with wax to avoid preferential orientation due to magnetic torque and to minimize the loss of crystallization solvent (when present) from the lattice. The resulting mixture was then inserted in an open-end quartz tube (0.80 mm outer diameter). To further reduce exposure to air, the tube was taken out of the glovebox in a sealed Schlenk, mounted on the sample holder rod under N$_2$ flux, precooled in a bath of liquid N$_2$, and inserted in the spectrometer at 100 K.

High-Frequency EPR powder spectra were recorded on a multifrequency spectrometer operating in a double-pass configuration. A 110 GHz frequency source (Virginia Diodes Inc.), associated with either a doubler or a tripler, was used. The propagation of this exciting light was performed with a quasi-optical bridge (Thomas Keating) outside the cryostat and with a corrugated waveguide inside it. The detection was carried out with a hot electron InSb bolometer (QMC Instruments). The main magnetic field was supplied by a 16 T superconducting magnet associated with a VTI (Cryogenic). The sample was prepared in a glovebox by thoroughly grinding large crystals of **2a**·4CHCl$_3$·2Et$_2$O immersed in a mixture of Et$_2$O and CHCl$_3$ (5:1 v/v) in an EPR tube, which was subsequently flame-sealed. The presence of the solvent allowed us to preserve the crystallinity and to prevent torqueing effects at low temperature. This preparation technique led to somewhat imperfect powder averaging, which, however, did not preclude a straightforward interpretation of the spectra. The powder spectra were simulated using parameters obtained through the fitting of the resonance positions.[59,60] Details on EPR experiments are given in Figures S31−S35.

Angular Overlap Model (AOM) Calculations. Ligand-field (LF) calculations within AOM[61] were performed using B, C, ζ_{3d}, and k values reported in refs 62 and 63. LF parameters were also taken from ref 62 and adapted to provide a reasonable reproduction of the electronic spectra reported in the literature for [Cr(4-Mepy)$_4$Cl$_2$].[62,64] This was achieved by considering a completely anisotropic π-interaction for the pyridine-type ligands and a completely isotropic π-interaction for the axial ligands X. Angular coordinates were either made to correspond to idealized D_4 point-group symmetry to study the dependency of the calculated D on axial and equatorial LF strength or were taken directly from X-ray structures. In the first case, the ring plane of each pyridine-type ligand was oriented so as to form a dihedral angle $\psi = 18°$ with the X−Cr−N$_{py}$ plane, in agreement with the structure of **2a**. For each ligand, $10Dq$ is defined as $3e_\sigma - 2e_{\pi s} - 2e_{\pi c}$.

DFT/CASSCF Calculations. DFT calculations were performed with the ORCA[65] program package, version 3.0.3.33 (see Figures S36−S38 for further information). The same computational setup used to optimize **2a** in the gas-phase[39] was applied to **1a**, **1b**, and **2b**. In detail, the PBE[66] functional with the D3 dispersion[67] correction scheme was used. Scalar relativistic recontracted versions of the Ahlrichs triple-ζ basis set, def2-TZVP, were chosen for Cr, N, and Cl atoms, while the single-ζ basis set, def2-SVP, was chosen for S, C, and H atoms.[68,69] Resolution of identity (RI) was used to approximate

two-electron integrals. Considering the possibility to face very flat potential energy surfaces, symmetric and unsymmetric arrangements of the Cr atoms were imposed as guess geometries. However, all geometries were fully optimized with no constraints on symmetry[47] or on the position of any Cr atom.[50] All the calculations were performed on a broken symmetry (BS) state with $S = 2$. A tight convergence threshold was also used (TightOpt). The SCF calculations were tightly converged (TightSCF) with unrestricted spin (UKS). Numerical integrations during all DFT calculations were done on a dense grid (ORCA grid4), while the final run was also performed on a denser one (ORCA grid5). Second-order anisotropy parameters (D, E) for the optimized unsymmetric structures of pentachromium(II) species **2a** and **2b** (**2a**$_{unsym}$ and **2b**$_{unsym}$) were computed at the *post*-HF (CASSCF) level. The use of *post*-HF approach is needed since the anisotropy tensor calculations at the UDFT level require the electronic spin density of the system to be consistent with an $\hat{S}^2$ eigenstate. Unfortunately, this is not the case since the value of $\langle\hat{S}^2\rangle$ from DFT significantly deviates from the expected spin-only value of 6 for a quintet state.[39] However, due to hardware computational limits, *post*-HF methods can only be applied to systems with a couple of magnetic centers and a reduced number of nonmagnetic atoms. For such a reason we chose a *divide et impera* approach by extrapolating two subunits from **2a**$_{unsym}$ and **2b**$_{unsym}$, namely, the monomer Cr1 and the dimer Cr2−Cr3, which represent the two basic units present in the lowest energy structure of pentachromium(II) strings. The Cr1 and Cr2−Cr3 models were obtained from optimized structures by simplifying the ligands to four pyridines and four (*E*)-*N*,*N*′-diethenylmethanimidamido ligands, respectively (Figure S38). Since the geometry of the Cr2−Cr3 fragment shows only negligible differences in **2a**$_{unsym}$ and **2b**$_{unsym}$, the Cr2−Cr3 model was based on **2a**$_{unsym}$. CASSCF calculations were done by employing a def2-TZVP basis set for Cr atoms and their first neighbors, while the def2-SVP basis set was used for all of the other atoms. The RI-J approximation along with the def2-TZVP/J auxiliary basis set for all the elements was used. Grids were set to 5 and VeryTightSCF. The use of def2-TZVP for all atoms showed no significant differences on the energy ladder of the excited states, thus supporting the choice of our computational setup.

RESULTS AND DISCUSSION

Synthesis and Structures. Trichromium(II) compounds **1a**·Et$_2$O and **1b**·0.4CH$_2$Cl$_2$ and pentachromium(II) compounds **2a**·4CHCl$_3$·2Et$_2$O and **2b** were synthesized by following (or by slight modification of) literature procedures.[33,34,41,43,46,52] Only **1b**·0.4CH$_2$Cl$_2$ is a new crystal phase and is the fourth published solvatomorph of **1b**, after **1b**· 2C$_6$H$_6$,[43] **1b**·2C$_7$H$_8$,[43] and **1b**·2C$_2$H$_4$Cl$_2$.[70] It was prepared by first reacting **1a**·Et$_2$O with TlBF$_4$ in CH$_3$CN to replace the axial chlorido ligands with CH$_3$CN, then precipitating the isothiocyanato derivative with KSCN, and finally recrystallizing it from CH$_2$Cl$_2$/*n*-hexane. The new method does not require isolation of a [Cr$_3$(dpa)$_4$(NCCH$_3$)$_2$]X$_2$ intermediate but results in comparable overall yield with respect to the published two-step synthesis of the benzene and toluene solvates.[43] The structure contains two-and-a-half trichromium-(II) complexes and one disordered interstitial molecule of dichloromethane per asymmetric unit.

Two Cr$_3$ moieties [molecule A: Cr1, Cr2, Cr3 (Figure 1); molecule B: Cr4, Cr5, Cr6] are entirely in general positions; the third one (molecule C: Cr7, Cr8, Cr7′) lies with its central metal site (Cr8) and two amido N atoms on a 2-fold axis and consequently has crystallographically imposed C_2 symmetry. When the central metal atom is modeled as a single, full-occupancy anisotropic scatterer (Model I), the three independent molecules in **1b**·0.4CH$_2$Cl$_2$ show a more or less symmetric arrangement of metal atoms, with Cr−Cr distances
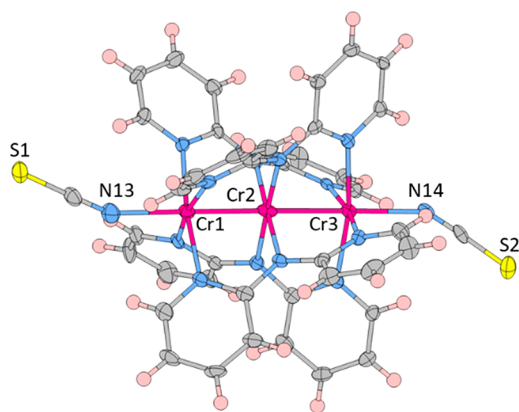
Figure 1. Structure of one of the independent molecules in **1b**·0.4CH$_2$Cl$_2$ (molecule A), in which the thermal ellipsoid of the central Cr^{2+} ion is distinctly prolate along the chain axis.

ranging from 2.31 to 2.36 Å (Table 1). Splitting of Cr2 in molecule A (Model II) gave Δd values typical of trichromium-(II) strings (0.23–0.30 Å).[43] The Cr–Cr–Cr moieties are linear within 2.5°, whereas the Cr-NCS units are bent at the N atom, with Cr–N$_{ax}$–C angles ranging from 144° to 165° (Table 1).

As a final remark, it is important to stress that the four EMACs under investigation have either idealized (**1a**·Et$_2$O, **1b**·0.4CH$_2$Cl$_2$, **2a**·4CHCl$_3$·2Et$_2$O) or crystallographic (**2b**) 4-fold symmetry. The analysis of the terminal chromophores (CrN$_4$Cl or CrN$_4$N) using program SHAPE v2.1[71] indeed indicates very small deviations from square-pyramidal (SPY-5) and vacant-octahedral (vOC-5) geometries, both of which have C_{4v} symmetry (Table S3). In chlorido derivatives the coordination spheres are closer to SPY-5, with shape measures ranging from 0.30 to 0.51, whereas in isothiocyanato-terminated strings deviation is minimal from vOC-5 (0.29–0.34).

Magnetic Measurements and EPR Spectra. The dc and ac magnetic measurements were performed on polycrystalline samples of **1a**·Et$_2$O, **1b**·0.4CH$_2$Cl$_2$, and **2b**. Compound **2a**·4CHCl$_3$·2Et$_2$O was studied both in solvated crystalline form and after solvent removal under vacuum. The solvated and unsolvated samples display very similar static and dynamic magnetic properties (see below). In an applied field of 1 kOe, the χT product of all compounds remains constant at 2.9–3.1 cm^3 K mol^{-1} between room temperature and 10–15 K, signaling a well-isolated $S = 2$ ground state. At lower temperatures, χT rapidly drops as expected from magnetic anisotropy effects. Isothermal molar magnetization (M) vs H data do not saturate at 70 kOe and 1.8–1.9 K, although the

highest obtained values (ca. 3.8 $N_A\mu_B$) are close to the expected saturation value for an $S = 2$ state ($4N_A\mu_B$ with $g = 2$). When plotted vs H/T, the magnetization curves display a pronounced nesting, suggesting deviation from the Brillouin function and the presence of magnetic anisotropy. The quantitative analysis of M vs H data (see Supporting Information for details) was based on zero-field-splitting (zfs) *plus* Zeeman Hamiltonian in eq 1:

$$\hat{H} = D[\hat{S}_Z^2 - S(S+1)/3] + E(\hat{S}_X^2 - \hat{S}_Y^2) + \mu_B\mathbf{B}\cdot\overline{\overline{\mathbf{g}}}\cdot\hat{\mathbf{S}}$$

(1)

where D and E are the axial and rhombic zfs parameters, respectively. **S** is the total spin vector, with component S_Z along the anisotropy axis (Z) (X, Y, and Z are the principal magnetic axes; as molecular symmetry is approximately 4-fold, Z must be close to the chain axis). For simplicity, rhombic anisotropy was disregarded ($E = 0$) and an isotropic Landé factor was assumed, i.e., $\overline{\overline{\mathbf{g}}} = g\overline{\overline{\mathbf{I}}}$, where $\overline{\overline{\mathbf{I}}}$ is the identity matrix. The best-fit anisotropy parameters so obtained (Table 2) confirm an easy-axis anisotropy ($D < 0$) for all compounds, with $|D| = 1.5$–1.7 cm^{-1} (the complete set of best-fit parameters is provided as Table S4).

For a more accurate, state-of-the-art determination of D and E, as well as of the principal components of the $\overline{\overline{\mathbf{g}}}$ matrix, we used W-band ($\nu \sim 94$ GHz) EPR spectroscopy. In spite of the difficulties in obtaining pure powder pattern spectra, the low temperature W-band EPR traces (Figure 2) provide an unequivocal picture over the trend of D values in the studied series of complexes. Because of the condition $|D| \sim h\nu$, the analysis of the spectra using eq 1 is not straightforward and requires careful consideration of the angular dependence of the transitions.[59] Most of them are actually occurring at off-axis turning points, the most intense one being close to 25 kOe, and as looping transitions (Figure S31). Only a couple of signals, expected to occur at 16 and 60 kOe for $D = -1.6$ cm^{-1}, $g = 1.99$, and $\nu = 94.27$ GHz, can be attributed to perpendicular transitions (Figure S32). The separation between these two lines (or the position of the first one, when the second exceeds the field range of the spectrometer, as occurring in **1b**·0.4CH$_2$Cl$_2$) shows that $|D|$ is slightly larger for tri- as compared to pentachromium(II) complexes and for isothiocyanato as compared to chlorido derivatives. On the other hand, the EPR transition observed around 25 kOe is essentially independent of the D value but can be used to obtain a more accurate estimate of $g_{X,Y}$, since it arises from microcrystallites oriented with their main anisotropy axes at $55° < \theta < 90°$ from the applied field (Figure S31).

With one exception, the observed experimental spectra indicate very weak rhombicity ($|E/D| \sim 0$), consistent with the

Table 2. Magnetic Parameters of Chromium(II)-Based EMACs with Different Nuclearity (n) and Axial Ligands (X), As Determined by EPR Spectroscopy and dc/ac Magnetic Measurements

compound	n	X	D (cm^{-1})[a]	$|E/D|$[a]	$g_{X,Y}$[a]	g_Z[a]	D (cm^{-1})[b]	U_{eff}/k_B (K)[c]	τ_0 (μs)[c]	ref
1a·CH$_2$Cl$_2$	3	Cl$^-$	−1.640[d]	0.021[d]	1.998[d]	1.981[d]		10.6(6)[e]	2.9(5)[e]	36, 37
1a·Et$_2$O	3	Cl$^-$	−1.66(5)	0.020(5)	2.000(5)	1.995(5)	−1.656(16)	10.5(5)[e]	3.1(5)[e]	this work
1b·0.4CH$_2$Cl$_2$	3	SCN$^-$	−1.78(5)	0.000(3)	1.998(3)	1.970(2)	−1.711(12)	12.4(5)[f]	0.26(5)[f]	this work
2a·4CHCl$_3$·2Et$_2$O	5	Cl$^-$	−1.53(1)	0.006(2)	1.990(3)	1.975(2)	−1.507(2)	8.6(5)[g]	11(5)[g]	35
2a	5	Cl$^-$					−1.510(6)	9.2(5)[g]	2.2(5)[g]	35
2b	5	SCN$^-$	−1.61(5)	0.003(2)	2.000(5)	1.985(2)	−1.696(4)	10.2(5)[g]	3.3(5)[g]	this work

[a]From W-band EPR, unless otherwise noted. [b]From isothermal M vs H data. [c]From ac susceptometry. [d]From high-frequency EPR (240 GHz). [e]Under an applied dc field of 2.0 kOe. [f]Under an applied dc field of 3.5 kOe. [g]Under an applied dc field of 2.5 kOe.
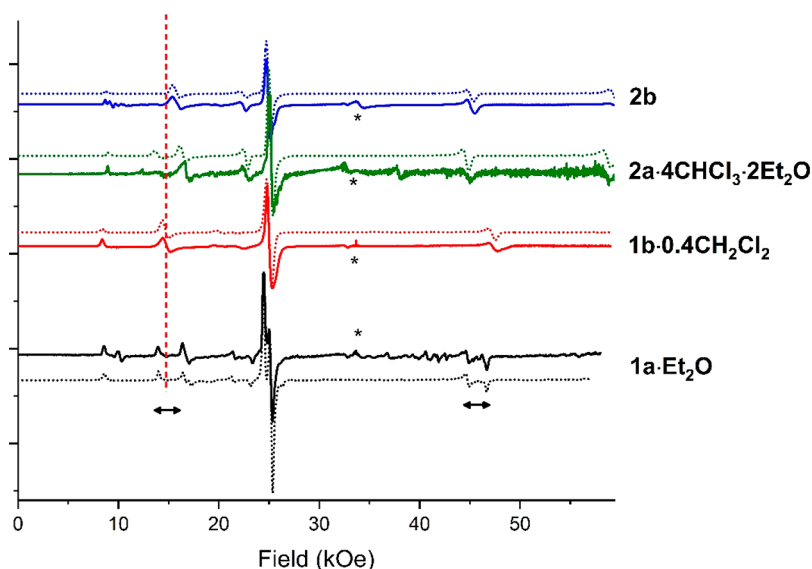
Figure 2. W-band (94.27 GHz) EPR spectra recorded at 6 K for **1a**·Et$_2$O, **1b**·0.4CH$_2$Cl$_2$, **2a**·4CHCl$_3$·2Et$_2$O, and **2b**. Continuous lines, experimental spectra; dotted lines, best simulations obtained using the parameters reported in the text. The double arrows evidence the splitting of the transitions due to the non-negligible rhombicity of **1a**·Et$_2$O. The vertical dashed line is centered on the perpendicular transition occurring furthest from the center of the spectrum, indicating the largest |D| value in the series. The asterisk indicates a signal from an impurity in the cavity walls. The spectrum of **2a**·4CHCl$_3$·2Et$_2$O and the corresponding simulation were originally reported in ref 35.

idealized or crystallographic 4-fold molecular symmetry. In **1a**·Et$_2$O, the 2-fold splitting of both perpendicular and looping transitions points to significant deviation from axiality. Following these considerations the spectra were simulated[72] to obtain the best-fit parameters gathered in Table 2 (an axial $\bar{\bar{g}}$ matrix was assumed to reduce the number of parameters). We stress that the evolution of the spectra at higher temperatures is only compatible with a negative D parameter (Figure S33), consistent with previous literature reports.[35–37] As for the rhombicity of **1a**·Et$_2$O, best simulations were obtained with |E/D| = 0.020(5), i.e., the same value reported for the dichloromethane solvate.[36,37] Unexpectedly, the inclusion of a small rhombic term was necessary to accurately reproduce the spectra of **2b**, suggesting that the actual molecular symmetry is lower than the reported crystallographic symmetry.[34] The $g_{X,Y}$ values are always very close to the free electron value, indicating a negligible effect of spin–orbit coupling over this parameter, whereas g_Z is always unequivocally smaller. Finally, the spectra of **1b**·0.4CH$_2$Cl$_2$ could be reproduced with a single set of spin Hamiltonian parameters. The structural differences among the three crystallographically independent molecules are thus undetectable by EPR.

For derivative **2a**·4CHCl$_3$·2Et$_2$O, the accuracy of the spin Hamiltonian parameters obtained from W-band EPR spectra was confirmed by a high-frequency EPR study at 220.8 and 331.2 GHz. The spectra show the pattern expected for an S = 2 spin system but some lines are split (Figures S34–S35). For instance, at 331.2 GHz the signal observed close to 7 T (M_S = −2 → −1 transition for the Z orientation) comprises a dominant and a satellite component at 6.93 and 6.96 T, respectively. The dominant peaks are consistent with the spin Hamiltonian parameters extracted from W-band spectra; their positions and those of the W-band signals were simultaneously fitted to give: D = −1.534(12) cm^{-1}, E = 0.008(5) cm^{-1}, g_X = 1.995(3), g_Y = 1.993(3), and g_Z = 1.985(11). The weaker signals, some of which *exceed* the highest fields of the dominant set, are attributed to a minority species (∼20% molar fraction)

with slightly different anisotropy parameters (D = −1.55 cm^{-1}, E = 0.011 cm^{-1}, g_X = 1.98, g_Y = 1.97, g_Z = 1.98), which remains unresolved in W-band spectra. The uncertainty on this second parameter set is larger because signals are weaker and fewer resonances can be identified; especially, no W-band signal could be introduced in the fit, thereby limiting the frequency range explored.

The ac magnetic susceptibility studies on all compounds revealed no out-of-phase component in zero dc field within the available range of temperature (down to 1.8 K) and frequency (up to 10 kHz). Application of a static field was however effective to reveal the magnetization relaxation leading to the appearance of an out-of-phase signal. The optimal field value (2.0–3.5 kOe) was located in a preliminary scan from 0 to 10 kOe at 1.8–1.9 K and was used for subsequent temperature and frequency dependent studies. Plots of lnτ vs 1/T were found to be linear in **1b**·0.4CH$_2$Cl$_2$, **2a**, and **2a**·4CHCl$_3$·2Et$_2$O, while a slight curvature was detected in **1a**·Et$_2$O and **2b**. Linear fits to all the data (or to the linear, high-temperature region) gave the effective anisotropy barriers (U_{eff}) and the attempt times (τ_0) gathered in Table 2. For all derivatives but **1b**·0.4CH$_2$Cl$_2$ the value of U_{eff} is, within uncertainty, coincident with the total splitting of the S = 2 multiplet ($U = |D|S^2$), as calculated from the D parameter determined by EPR and when accounting for an external dc field. We note in this respect that **1b**·0.4CH$_2$Cl$_2$ shows the widest distribution of relaxation times (α) at the measuring field. This has recently been shown[73] to result in a large uncertainty on the actual relaxation time and thus on the parameters of the relaxation process. We can then conclude that all the data lend support to an overbarrier Orbach mechanism for magnetic moment reversal.

In spite of the small S value, all chromium(II)-based EMACs considered in this and previous works[35,36] behave as SMMs, although the observation of magnetic bistability by ac susceptibility measurements requires the application of a dc magnetic field. In this respect, their magnetic properties are similar to those of the mononuclear square planar complexes

Table 3. Magnetic Parameters for Terminal Ion (Cr1) in Chromium(II)-Based EMACs with Different Nuclearity (n) and Axial Ligands (X), Evaluated within the AOM[a]

	n, X	D (cm^{-1})[b]	D (cm^{-1})[c]	E (cm^{-1})[b]	g_X[b]	g_Y[b]	g_Z[b]	ref
1a·Et$_2$O	3, Cl$^-$	−1.42	−0.61	0.010	1.998	1.998	1.978	this work
1b·0.4CH$_2$Cl$_2$[d]	3, SCN$^-$	−1.55	−0.61	5 × 10^{-3}	1.998	1.998	1.977	this work
2a·4CHCl$_3$·2Et$_2$O	5, Cl$^-$	−1.44	−0.61	6 × 10^{-3}	1.998	1.998	1.978	this work, 35
2b	5, SCN$^-$	−1.60	−0.64	0	1.998	1.998	1.976	this work

[a]LF parameters: $B = 800$ cm^{-1}, $C = 3300$ cm^{-1}, $\zeta_{3d} = 235$ cm^{-1}, $k = 0.82$, $10Dq(N) = 16500$ cm^{-1}, $10Dq(Cl^-) = 5000$ cm^{-1}, $10Dq(SCN^-) = 8000$ cm^{-1}, $(e_{\pi c} + e_{\pi s})/e_\sigma = 0.3$ for all ligands, $e_{\pi c}(N)/e_{\pi s}(N) = 0.0$, $e_{\pi c}(X)/e_{\pi s}(X) = 1.0$ (X = Cl$^-$, SCN$^-$). [b]Calculated by including all the states arising from 3d^4 configuration. [c]Calculated by considering only states arising from ^{5}D term. [d]Calculated for molecule C (Cr7, Cr8, Cr7′) with crystallographic C_2 symmetry.
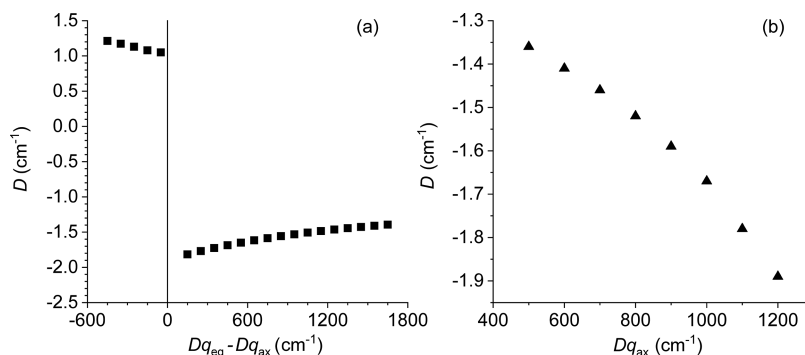

Figure 3. Calculated D value for a 3d^4 ML$_4$X$_2$ system in D_4 symmetry: (a) as a function of the difference between equatorial and axial LF strength $[(e_{\pi c} + e_{\pi s})/e_\sigma = 0.3$ for all ligands, $e_{\pi c}^{eq}/e_{\pi s}^{eq} = 0$, $e_{\pi c}^{ax}/e_{\pi s}^{ax} = 1]$; (b) as a function of axial LF strength for constant $e_{\pi c}^{ax} = e_{\pi s}^{ax} = 312.5$ cm^{-1}, $(e_{\pi c}^{eq} + e_{\pi s}^{eq})/e_\sigma^{eq} = 0.3$, $e_{\pi c}^{eq}/e_{\pi s}^{eq} = 1$. For both plots the other parameters were: $B = 800$ cm^{-1}, $C = 3300$ cm^{-1}, $\zeta_{3d} = 235$ cm^{-1}, $k = 0.82$, and $Dq_{eq} = 1650$ cm^{-1}.

[Cr{N(SiMe$_3$)$_2$}$_2$(py)$_2$] and [Cr{N(SiMe$_3$)$_2$}$_2$(THF)$_2$], which also feature a negative D value, very weak rhombicity, and slow relaxation of their magnetization observed under dc field.[74]

Angular Overlap Model Calculations. The angular overlap model (AOM)[61] proved remarkably successful in predicting the anisotropy of 2a·4CHCl$_3$·2Et$_2$O starting from the coordination environment of its structurally isolated terminal ion.[35] We herein show that the same approach offers a straightforward explanation of the slightly enhanced anisotropy observed in the isothiocyanato derivative 2b. Calculations were performed starting from the experimental atomic coordinates of 2a·4CHCl$_3$·2Et$_2$O and 2b and using the same ligand-field (LF) parameters as reported in ref 35 (except for a larger Dq value for SCN$^-$ compared to Cl$^-$, in agreement with their relative position in the spectrochemical series). The calculated g values are in accordance with EPR spectra, with $g_{X,Y}$ very close to 2.00 and g_Z always around 1.98 (Table 3). More important, the resulting D parameters quantitatively agree with the experimental results, including the larger $|D|$ value of 2b. The role of excited triplet states emerges clearly from side calculations in which triplets are disregarded; in this case, the $|D|$ parameters are dramatically underestimated (ca. 0.6 vs 1.4−1.6 cm^{-1}), and the differences between the two complexes become negligible (Table 3).

These results are easily rationalized by analyzing idealized tetragonal structures containing four equatorial pyridine-type ligands and two weaker axial ligands (i.e., $Dq_{ax} < Dq_{eq}$). When the LF parameters of equatorial sites are held fixed, the D value is crucially determined by the global LF strength of the two axial coordination sites, i.e., by the sum of their Dq values. In particular, as the average Dq of axial ligands is increased toward that of equatorial ligands, i.e., on lowering distortions from octahedral symmetry, the AOM predicts a more negative D value (Figure 3a). While this might look counterintuitive, one

has to consider that the 3d^4 configuration in octahedral symmetry is characterized by a ^5E_g ground state, which cannot be mapped on a simple spin Hamiltonian such as eq 1, even including higher-order terms. However, as soon as the octahedral degeneracy is lifted by tetragonal elongation, the spin Hamiltonian formalism can be applied; in a perturbative approach the magnitude of $|D|$ is then inversely dependent on the extent of distortion.[75] This effect is triggered primarily by the strength of the σ interaction with the axial ligand(s) (see Figure 3b). Furthermore, it crucially depends on the contribution of excited triplet states, which takes the form:[76,77]

$$D' = -\frac{\zeta_{3d}^2/4}{6B + 5C - \Delta E} \quad (2)$$

where ζ_{3d} is the single 3d-electron spin−orbit coupling constant, B and C are Racah parameters, and

$$\Delta E \cong 2e_\sigma^{ax} + e_\sigma^{eq} - 2e_\pi^{ax} - 2e_\pi^{eq} \quad (3)$$

is the energy difference between the 3d$_{z^2}$ orbital and the 3d$_{xz}$, 3d$_{yz}$ pair for isotropic π interactions [please note that eq 2 was misprinted in ref 78]. From eq 3, it follows that ΔE increases with increasing σ donor strength of the axial ligands, causing D' to become more negative (eq 2). By contrast, the contribution of quintet states is smaller[79] and independent of e_σ^{ax}, while singlets essentially do not contribute to the anisotropy.

In trichromium(II) strings (1a and 1b), the coordination environment of terminal ions remains quite similar to their longer congeners and, rather unsurprisingly, AOM predicts comparable single-ion anisotropies and g factors (Table 3). Based on the available experimental and theoretical knowledge, however, the origin of magnetic anisotropy in 1a and 1b is much less straightforward. While chlorido derivative 2a entails

a fairly isolated Cr1 center and two formally diamagnetic chromium(II) pairs,[39] the ground structure of **1a** is symmetric.[46] Therefore, contributions to magnetic anisotropy potentially arise from both terminal ions as well as from central ion. One might reason that three localized $s = 2$ spins with strong antiferromagnetic coupling would also yield a well-isolated $S = 2$ ground state, whose D parameter relates to projected single-ion anisotropies.[80] At this stage, shedding light on the origin of magnetic anisotropy clearly requires a more accurate electronic description of these EMACs based on *ab initio* methods. The DFT/CASSCF calculations described in the next section indeed disprove a spin-localized model of trichromium(II) strings, while providing a simple explanation as to why the two types of strings have similar magnetic anisotropy.

DFT Structure Optimization. In our *ab initio* investigation of **1a**, **1b**, **2a**, and **2b**, the Cr centers were numbered as Cr1, Cr2, ⋯, Cr5 along the chain, with Cr1 representing the formally "isolated" metal center in the unsymmetric structures. The results of structural optimization on **2a** were published in ref 39 where we probed the two different energy minima corresponding to a symmetric (**2a**$_\text{sym}$) and an unsymmetric (**2a**$_\text{unsym}$) structure (these data are collected in Table 4 for

Table 4. Computed Cr−Cr Distances (Å) in the Symmetric and Unsymmetric Structures of 2a and 2b (BS $S = 2$ state)

	X	Cr1−Cr2	Cr2−Cr3	Cr3−Cr4	Cr4−Cr5	ref
2a$_\text{sym}$	Cl⁻	2.319	2.207	2.221	2.308	39
2b$_\text{sym}$	SCN⁻	2.285	2.246	2.246	2.285	this work
2a$_\text{unsym}$	Cl⁻	2.550	1.862	2.606	1.904	39
2b$_\text{unsym}$	SCN⁻	2.547	1.865	2.604	1.908	this work

convenience). In agreement with the structural model proposed by Cotton et al.,[38,81] the unsymmetric structure was found more stable by 2.9 kcal mol⁻¹.[39] The same calculation protocol applied to **2b** gave a similar energy profile, with **2b**$_\text{unsym}$ more stable than **2b**$_\text{sym}$ by 1.7 kcal mol⁻¹, and the overall geometrical parameters were in close agreement with the experimental structure (including perfectly linear Cr-NCS units). These results confirm the occurrence of a shallow potential energy surface in both pentachromium(II) species. Furthermore, terminal ligands have little influence on the geometry of both symmetric and unsymmetric structures. For instance, the two inner Cr−Cr distances in **2a**$_\text{sym}$ (Cr2−Cr3 and Cr3−Cr4) are shorter (2.21−2.22 Å) than those for Cr1−Cr2 and Cr4−Cr5 (2.31−2.32 Å) (see Table 4).[39] The pattern is similar in **2b**$_\text{sym}$, albeit with a smaller difference between the two sets of distances (2.25 Å for inner and 2.28 Å for outer Cr−Cr separations). Notice that a Cr−Cr distance of ~2.2 Å corresponds to a multiple bond.[82]

In the unsymmetric structures, the C_2 symmetry element located on Cr3 is lost and an alternation of short and long distances is found, with $d_<$ = 1.86−1.91 Å and $d_>$ = 2.55−2.61 Å (see Table 4). It is worth mentioning that Cr−Cr distances of 1.8−1.9 Å are in agreement with a third/fourth-order Cr−Cr bond,[82] while a very weak Cr−Cr interaction is expected for distances longer than ~2.5 Å. Such results strongly suggest that one of the terminal Cr²⁺ ions in the most stable, unsymmetric structure of pentachromium-(II) strings can be considered as "isolated" and with a square-pyramidal coordination environment featuring the Cl⁻ or SCN⁻ ligands in apical position.

The computed spin densities (Löwdin analysis) and expectation values $\langle \hat{S}^2 \rangle$ for the BS $S = 2$ state, reported in Table 5, are very similar for corresponding structures of **2a** and **2b**. On average, the spin densities in **2b** are slightly reduced as compared with **2a** while $\langle \hat{S}^2 \rangle$ is practically unchanged.

The alternating signs and the magnitudes of the spin densities support the goodness of the BS solution obtained for $S = 2$ and, in addition, evidence the impact of an unsymmetric versus symmetric configuration on the electronic structure. Indeed, in the symmetric structures the spin densities are almost homogeneous in absolute value among the five metal centers (3.0−3.1 unpaired electrons on Cr1 and Cr5; 2.4−2.6 unpaired electrons on Cr2, Cr3, and Cr4). On the contrary, in the unsymmetric structures 3.3−3.4 unpaired electrons are localized on Cr1 while only 1.4−1.7 unpaired electrons are present on each of the remaining metal centers. The amount of spin density left on Cr2, Cr3, Cr4, and Cr5 suggests that a bond order larger than three is unlikely to occur within the formally quadruply bonded Cr2−Cr3 and Cr4−Cr5 pairs, while a practically isolated Cr1 is confirmed. Therefore, a bond localization is clearly evident compared to the symmetric case.

The expectation value $\langle \hat{S}^2 \rangle$ calculated by DFT gives an indication of the closeness of the spin ground state of a molecule to the multispin picture suggested by the atomic spin density values.[83,84] The latter suggest the presence of antiferromagnetically coupled spins along the chain. In an unrestricted DFT formalism this should correspond to an $\langle \hat{S}^2 \rangle$ calculated value of 10.81 (10.69) for **2a**$_\text{sym}$ (**2b**$_\text{sym}$) and 8.83 (8.78) for **2a**$_\text{unsym}$ (**2b**$_\text{unsym}$).[83,84] In all cases, the calculated values reported in Table 5 are underestimated. This points to a deviation from a multispin picture and the presence of significant overlap between the orbitals bearing the unpaired spins. Moreover, this effect is stronger in the unsymmetric case, further supporting the previous analysis in terms of spin densities and bond lengths.

The structure optimization procedure was extended to trichromium(II) species **1a** and **1b** (Table 6). In agreement with previous studies,[46−51] the energy difference between **1a**$_\text{unsym}$ and **1a**$_\text{sym}$ is now 5.4 kcal mol⁻¹, but in favor of the symmetric structure. Unfortunately, it was not possible to fully

Table 5. Computed Spin Densities[a] and $\langle \hat{S}^2 \rangle$ Values in the Symmetric and Unsymmetric Structures of 2a and 2b (BS $S = 2$ state)

	X	Cr1	Cr2	Cr3	Cr4	Cr5	$\langle \hat{S}^2 \rangle$	ref
2a$_\text{sym}$	Cl⁻	3.10	−2.45	2.50	−2.44	3.12	10.46	39
2b$_\text{sym}$	SCN⁻	3.01	−2.39	2.60	−2.37	3.01	10.41	this work
2a$_\text{unsym}$	Cl⁻	3.40	−1.40	1.60	−1.54	1.73	8.04	39
2b$_\text{unsym}$	SCN⁻	3.31	−1.40	1.62	−1.52	1.71	8.03	this work

[a]In unpaired electrons.

Table 6. Computed Cr−Cr Distances (Å), Spin Densities,[a] and $\langle\hat{S}^2\rangle$ Values in the Symmetric and Unsymmetric Structures of 1a and 1b (BS S = 2 state)

|	X	Cr1−Cr2	Cr2−Cr3	Cr1	Cr2	Cr3	$\langle\hat{S}^2\rangle$
1a$_{sym}$	Cl$^-$	2.335	2.335	3.17	−2.54	3.17	8.38
1b$_{sym}$	SCN$^-$	2.337	2.337	3.18	−2.56	3.18	8.41
1a$_{unsym}$	Cl$^-$	2.686	1.886	3.50	−1.52	1.79	7.08
1b$_{unsym}$	SCN$^-$	−	−	−	−	−	−

[a]In unpaired electrons.

converge on an unsymmetric structure for isothiocyanato derivative **1b** because the optimization procedure kept on converging on a symmetric one. At any rate, such behavior hints to symmetric and unsymmetric structures of very similar energy, with a slight preference for the symmetric one.

The spin densities and $\langle\hat{S}^2\rangle$ values are also presented in Table 6. Also in this case, the DFT calculated $\langle\hat{S}^2\rangle$ values deviate from those expected from the multispin picture (8.44, 8.46, and 7.41 for **1a$_{sym}$**, **1b$_{sym}$**, and **1a$_{unsym}$**, respectively) confirming that trichromium(II) strings cannot be described as three localized, exchange-coupled s = 2 spins.[83,84] To further support our analysis, we calculated the exchange-coupling constants between Cr^{2+} ions in **1a$_{sym}$** at the BS-DFT level (see the Supporting Information for more details).[83] Use of the spin Hamiltonian $\hat{H} = J_1(\hat{s}_1 \cdot \hat{s}_2 + \hat{s}_2 \cdot \hat{s}_3) + J_2\hat{s}_1 \cdot \hat{s}_3$, where s_i is the spin vector localized on Cri, gives large antiferromagnetic interactions between nearest neighbors (J_1 = 1635 cm^{-1}) and next-nearest neighbors (J_2 = 606 cm^{-1}), clearly indicating the presence of a delocalized bond all over the three Cr^{2+} ions. We conclude that, in the gas phase, the preferred geometry of the investigated tri- and pentachromium(II) species with terminal Cl$^-$ or SCN$^-$ ligands is symmetric and unsymmetric, respectively.

Electronic Structures. We analyzed in greater detail the electronic structures of the chlorido derivatives **1a** and **2a** through the use of quasi-restricted molecular orbitals (QROs), computed at the DFT level.[85] Figures 4 and 5 depict the singly occupied QROs (SOMOs) for the optimized unsymmetric and symmetric structures of **2a** and **1a**, respectively (from now on, the principal quantum number will be dropped from orbital symbols, unless when strictly necessary). In **2a$_{unsym}$**, these four frontier QROs have strong d-like character (d$_{xy}$, d$_{xz}$, d$_{yz}$, and d$_{z^2}$) and are well localized on Cr1 (Figure 4). The d$_{x^2-y^2}$-like orbital is found at higher energy and is empty (VIRTUAL). Such a result suggests that the unsymmetric structures can be considered as the superposition of two subunits, Cr1 and Cr2−Cr3−Cr4−Cr5, marginally interacting with each other. Indeed, only the d$_{z^2}$-like QRO on Cr1 is slightly delocalized over the Cr2−Cr3−Cr4−Cr5 fragment, as expected since the d$_{z^2}$ metal orbitals have the most efficient overlap along the metal chain. Turning now to the Cr2−Cr3−Cr4−Cr5 fragment, the $\sigma(\sigma^*)$ interactions are delocalized over the four ions, whereas $\pi(\pi^*)$ and $\delta(\delta^*)$ interactions are pretty localized on the Cr2−Cr3 and Cr4−Cr5 pairs, as suggested by the computed short Cr−Cr distances (Figure S36).

Considering a symmetric structure (**2a$_{sym}$**) of the complex, a completely different picture would result (Figure S37). The unpaired electrons would now be found in four QROs (SOMOs) which can be described as one σ, two π, and one δ nonbonding linear combinations of metal d orbitals. Nodal planes are present on Cr2 and Cr4 in all four QROs except for σ molecular orbital, where some electron density is still present on Cr2 and Cr4. A fifth δ-type nonbonding combination, with

$d_{x^2-y^2}$ (VIRTUAL)

d_{z^2} (SOMO)

d_{xz} (SOMO) d_{yz} (SOMO)

d_{xy} (SOMO)
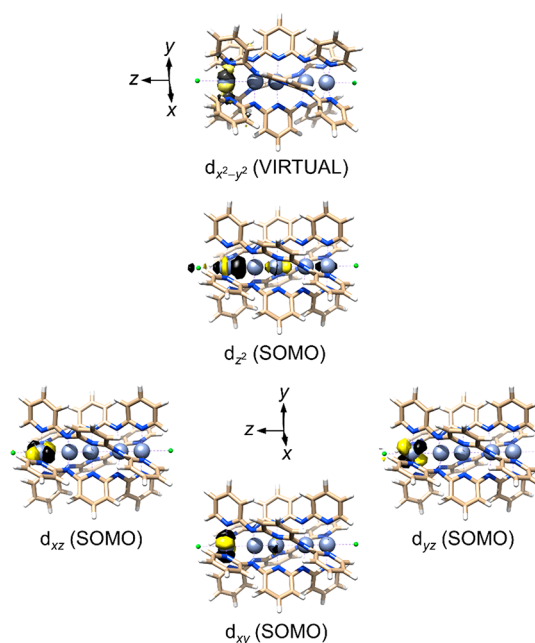
Figure 4. Frontier QROs in **2a$_{unsym}$**. The given reference frame is used to label the d-like QROs, which are almost completely localized on the leftmost Cr^{2+} ion (Cr1). A slightly different molecular orientation is used for a better representation of the d$_{x^2-y^2}$-like QRO. Positive and negative signs of the wave function are plotted in yellow and black, respectively.

contributions from odd sites only, remains unoccupied (VIRTUAL); it was included in Figure S37 for consistency with the composition of SOMOs, although it is not the LUMO. The four unpaired electrons in **2a$_{sym}$** are thus *shared* among Cr1, Cr3, and Cr5, whereas they are *localized* on Cr1 in **2a$_{unsym}$**. However, the presence of a nodal plane on Cr2 and Cr4 makes each terminal Cr^{2+} ion in **2a$_{sym}$** almost equivalent to Cr1 in **2a$_{unsym}$** *in terms of electronic structure*.

A scenario similar to **2a$_{sym}$** occurs in trichromium(II) string **1a$_{sym}$**. The four unpaired electrons are in one σ, two π, and one δ nonbonding linear combinations of d orbitals centered on Cr1 and Cr3 (SOMOs), with a nodal plane now located on central metal Cr2 (Figure 5). A fifth δ-type molecular orbital also delocalized on Cr1 and Cr3 is found at higher energy and is empty (VIRTUAL); although it is not the LUMO, it was included in our analysis for symmetry consistency with the composition of the SOMOs.

Since the Cr1N$_4$ and Cr3N$_4$ basal planes are twisted by ∼45° with respect to each other along the chain axis, the wave function composition in terms of d orbitals can be worked out by simple inspection of Figure 5:

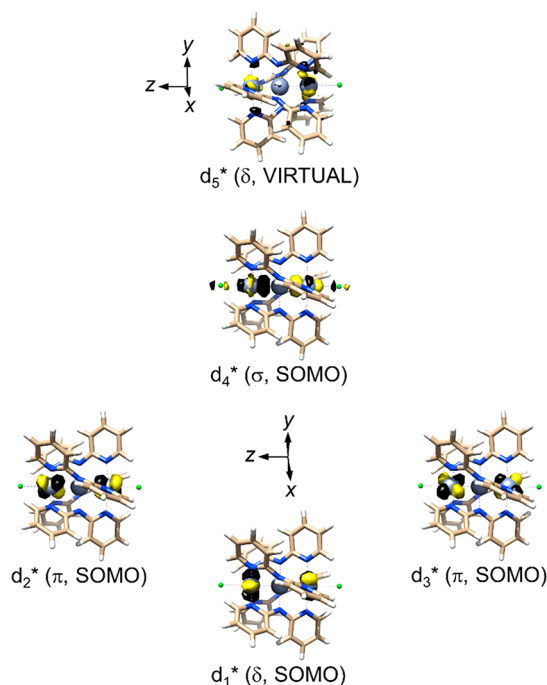$$d_1^* = 2^{-1/2}(d_{xy}^{Cr1} - d_{x^2-y^2}^{Cr3}) \tag{4a}$$

Figure 5. Frontier QROs in $1a_{sym}$. The reference frame is defined by the coordination environment of Cr1 and is used to label the d-like contributions to QROs, as given by eqs 4a−4e. A slightly different molecular orientation is used for a better representation of d_5^*. Positive and negative signs of the wave function are plotted in yellow and black, respectively.

$$d_2^* = 2^{-1/2}(d_{yz}^{Cr1} - d_{yz}^{Cr3}) \tag{4b}$$

$$d_3^* = 2^{-1/2}(-d_{xz}^{Cr1} + d_{xz}^{Cr3}) \tag{4c}$$

$$d_4^* = 2^{-1/2}(-d_{z^2}^{Cr1} + d_{z^2}^{Cr3}) \tag{4d}$$

$$d_5^* = 2^{-1/2}(-d_{x^2-y^2}^{Cr1} - d_{xy}^{Cr3}) \tag{4e}$$

Notice that d orbitals on Cr1 and Cr3 are expressed in two collinear reference frames, whose orientation is defined by the coordination environment of Cr1 (see Figure 5 and the Supporting Information for more details). These results provide a starting point to explain the similar magnetic behavior observed in tri- and pentachromium(II) derivatives, in spite of their different structural preferences and electronic structure.

The Origin of Magnetic Anisotropy. The "isolated" Cr^{2+} ion (Cr1) in the ground, unsymmetric structures of pentachromium(II) strings ($2a_{unsym}$ and $2b_{unsym}$) displays a square-pyramidal coordination environment, with the metal only slightly out of the basal plane. Calculations at CASSCF-(4,5) level on truncated Cr1 models (Figure S38a,b) afford an easy-axis anisotropy in the ground quintet state, with $D = -1.513$ and -1.592 cm^{-1} in $2a_{unsym}$ and $2b_{unsym}$, respectively (see Table 7).

These CASSCF results compare well with the experimental data gathered in Table 2 and with the predictions of AOM (Table 3) and correctly reproduce the larger axial anisotropy of the isothiocyanato (**2b**) versus chlorido (**2a**) derivative.

To check the validity of the truncated models, we also calculated the magnetic properties of the neighboring Cr2−Cr3 pair (Figure S38c). As suggested by the short Cr−Cr

Table 7. Magnetic Parameters (cm^{-1}) Determined by CASSCF Calculations on Cr1 and Cr1Zn$_4$ Models of $2a_{unsym}$ and $2b_{unsym}$

model	$2a_{unsym}$ (X = Cl$^-$)		$2b_{unsym}$ (X = SCN$^-$)	
	D	E/D	D	E/D
Cr1	−1.513	0.000	−1.592	0.000
Cr1Zn$_4$	−1.441	0.000	−1.248	0.000

distance and confirmed by the computed unrestricted natural orbitals (UNOs), the two chromium(II) ions are strongly coupled, and for this reason, both static and dynamic correlations are supposed to be relevant. Therefore, CASSCF-(8,8) was used to determine the electronic structure for this fragment. The active space was built with σ; π; π; δ and σ*; π*; π*; δ* orbitals (derived from the combination of d orbitals except for $d_{x^2-y^2}$), and the wave function was allowed to converge on both the first triplet and singlet solutions. As expected, the singlet state was found more stable by 3927.95 cm^{-1}, indicating that the Cr2−Cr3 unit can be regarded as a diamagnetic fragment. UNO analysis gave a bond order of 2.27 for the singlet ground state solution, which significantly deviates from the expected value of 4. As reported in literature,[50] this is due to the partial occupation of antibonding orbitals as an effect of electron correlation. The twist of neighboring equatorial N$_4$ planes results in a deviation from a perfectly eclipsed configuration,[86] which reduces the overlap between d_{xz}, d_{yz}, and d_{xy} orbitals, i.e., the ones responsible for π and δ interactions. In turn, this effect leads to a lower energy splitting between their bonding and antibonding combinations, causes a larger spread of electron occupation numbers all over the Fermi energy region, and reduces the effective bond order of the chromium pair. According to the above considerations, the Cr2−Cr3−Cr4−Cr5 unit is expected to behave as a diamagnetic fragment and to only marginally affect the electronic structure of Cr1. Moreover, the long Cr1−Cr2 distance and the almost complete separation between UNOs of the two different fragments strongly suggest that the magnetic behavior of these unsymmetric EMACs is ruled *only by the Cr1 fragment*.

To further evaluate the effect of the Cr2−Cr3−Cr4−Cr5 fragment on the D value of Cr1, we performed a CASSCF calculation replacing the four Cr^{2+} with Zn^{2+} ions, without any structural relaxation (Cr1Zn$_4$ model). Such a choice was necessary since the explicit inclusion of the four Cr^{2+} ions would be computationally too demanding. The magnetic anisotropy parameters for Cr1 and Cr1Zn$_4$ models based on the structures of $2a_{unsym}$ and $2b_{unsym}$ are compared in Table 7. The Zn^{2+} ions have a limited impact on calculated D values, which become somewhat less negative. We can therefore conclude that an axial "diamagnetic substitution" approach does not significantly alter the main contributions to the anisotropy, which originate almost totally from the N$_4$Cl or N$_4$N coordination environments.

Unfortunately, CASSCF calculations cannot be applied to the symmetric structure of trichromium(II) complexes; for a correct representation of their electronic structure, the CAS space should be extended over the 3d sets of the three Cr^{2+} ions, and this would be unmanageable in terms of computational resources.

A unified treatment of both types of complexes can however rely on an approach devised by Neese et al.,[85,87,88] in which the electronic structure is described in terms of QROs. For

simplicity, we herein limit our analysis to the d-like molecular orbitals that are depicted in Figures 4 and 5 and whose energies, as provided by DFT/PBE calculations, are reported in Table 8. As discussed above, in $2a_{unsym}$ and $2b_{unsym}$ these

Table 8. Calculated Frontier d QRO Eigenvalues (eV) for $1a_{sym}$, $1b_{sym}$, $2a_{unsym}$, and $2b_{unsym}$

	$1a_{sym}$		$1b_{sym}$	
	ε^{α}	ε^{β}	ε^{α}	ε^{β}
d_1^* (SOMO)	−4.694	−1.769	−4.915	−2.032
d_2^* (SOMO)	−4.422	−1.460	−4.605	−1.759
d_3^* (SOMO)	−4.422	−1.460	−4.605	−1.759
d_4^* (SOMO)	−3.429	−1.294	−3.501	−1.334
d_5^* (VIRTUAL)	−1.628	−^{a}	−1.918	−^{a}
	$2a_{unsym}$		$2b_{unsym}$	
	ε^{α}	ε^{β}	ε^{α}	ε^{β}
d_{xy}^{Cr1} (SOMO)	−4.705	−1.828	−4.846	−2.031
d_{xz}^{Cr1} (SOMO)	−4.495	−1.334	−4.595	−1.587
d_{yz}^{Cr1} (SOMO)	−4.494	−1.333	−4.594	−1.586
$d_{z^2}^{Cr1}$ (SOMO)	−3.649	−1.618	−3.662	−1.651
$d_{x^2-y^2}^{Cr1}$ (VIRTUAL)	−1.583	−^{a}	−2.019	−^{a}

^{a}Not reported since not needed in calculations.

frontier QROs essentially correspond to the d orbitals of Cr1 (Figure 4). Notice that their energy ordering for α spin components is consistent with the square-pyramidal coordination geometry of Cr1, namely:

$$\varepsilon^{\alpha}(d_{xy}^{Cr1})^1 < \varepsilon^{\alpha}(d_{xz}^{Cr1})^1 = \varepsilon^{\alpha}(d_{yz}^{Cr1})^1 < \varepsilon^{\alpha}(d_{z^2}^{Cr1})^1 < \varepsilon^{\alpha}(d_{x^2-y^2}^{Cr1})^0 \qquad (5)$$

where we have included information on electronic occupation as superscript. The contribution of quintet and triplet excited states to the axial zfs parameter (D) of the ground $S = 2$ state is then described in terms of single-particle $\alpha \rightarrow \alpha$ (SOMO → VIRTUAL) and $\alpha \rightarrow \beta$ (SOMO → SOMO) spin excitations, respectively (details are available in the Supporting Information). The values of $D_{\alpha\rightarrow\alpha}$, $D_{\alpha\rightarrow\beta}$, and $D = D_{\alpha\rightarrow\alpha} + D_{\alpha\rightarrow\beta}$ obtained by setting the 3d spin−orbit coupling constant (ζ_{3d}) for Cr^{2+} to the free-ion value are presented in Table 9. Such results are only semiquantitative since several other excitations involving doubly occupied and empty orbitals, as well as spin−spin contributions, were not included.[88]

Table 9. Calculated Values of $D_{\alpha\rightarrow\alpha}$, $D_{\alpha\rightarrow\beta}$, and Overall D (cm^{-1}) with $\zeta_{3d} = 230$ cm^{-1}

	$1a_{sym}$	$1b_{sym}$	$2a_{unsym}$	$2b_{unsym}$
$D_{\alpha\rightarrow\alpha}$	−0.46	−0.47	−0.38	−0.42
$D_{\alpha\rightarrow\beta}$	−1.18	−1.25	−1.30	−1.36
D	−1.64	−1.72	−1.68	−1.79

Table 9 clearly shows that spin-forbidden ($\alpha \rightarrow \beta$) LF excitations can by no means be neglected. From the relevant equations reported in the Supporting Information, it is seen that the $D_{\alpha\rightarrow\alpha}$ contribution becomes more negative as d_{xy} and $d_{x^2-y^2}$ get closer in energy. Considering σ interactions as dominant, this condition is fulfilled on lowering the σ LF contributions of the equatorial ligands. On the other hand, $D_{\alpha\rightarrow\beta}$ contribution becomes more negative if the α (β) component of d_{z^2} and the β (α) component of d_{xz}/d_{yz} pair get closer in energy, i.e., on increasing the axial LF strength given by the terminal ligand and by the Cr2−Cr3−Cr4−Cr5

fragment. All these considerations are in agreement with the results obtained in AOM section and with previous work on other isoelectronic systems.[75−79,89]

In the case of $1a_{sym}$ and $1b_{sym}$, frontier QROs are no longer single-center d orbitals, although they exhibit a similar energy pattern to pentachromium(II) strings (Table 8). With the wave functions given by eqs 4a−4e and the corresponding spin-resolved energies (Table 8), Neese's approach yields the $D_{\alpha\rightarrow\alpha}$, $D_{\alpha\rightarrow\beta}$, and overall D parameters also presented in Table 9 (details are available in the Supporting Information).

These data give numerical support to the similar anisotropy displayed by tri- and pentachromium(II) derivatives, primarily because frontier MOs with dominant d character follow a similar energy pattern. The ultimate reason is that frontier orbitals in trichromium(II) chains are nonbonding linear combinations of d orbitals of Cr1 and Cr3, and their energy thus largely reflects the d-level pattern of terminal ions. Furthermore, our treatment also accounts for the slightly enhanced anisotropy of isothiocyanato versus chlorido derivatives.

■ CONCLUSION

The present work is the first systematic attempt to extend magnetic studies on odd-membered ($n = 3, 5$) chromium(II)-based EMACs beyond S-value determination. As a first important result, we found that both tri- and pentachromium-(II) strings have a negative zfs parameter D ($|D| = 1.5−1.8$ cm^{-1}), weak rhombicity ($|E/D| \leq 0.02$), and display slow relaxation of their magnetization. These properties are only marginally affected by the axial ligands ($X = Cl^-$, SCN^-), with the isothiocyanato derivatives slightly more anisotropic than the chlorido complexes. Such similarities in electronic structure over remarkably small energy scales are surprising in light of the different structural preferences as chain length is varied. Confirming previous experimental and theoretical investigations,[39,46−51] our DFT calculations showed that the preferred structure is symmetric (D_4) for $n = 3$ but unsymmetric (C_4) for $n = 5$. The subsequent step of our work then consisted in investigating the impact of a symmetric versus unsymmetric structure on the distribution of unpaired electrons and on the zfs of the $S = 2$ state. DFT studies on pentachromium(II) complexes clearly showed the occurrence of a structurally isolated terminal Cr^{2+} ion (Cr1), whose d orbitals provide the leading contribution to the four SOMOs. CASSCF-level calculations on terminal Cr1N$_4$Cl and Cr1N$_4$N chromophores in fact yielded D and E parameters in remarkable agreement with experiment and with elementary LF arguments based on the spectrochemical series.

Such a structural confinement is absent in the symmetric structure of trichromium(II) strings, whose terminal metals are equivalent by symmetry. However, a major simplification arises from the fact that, to a good approximation, the four SOMOs are nonbonding linear combinations of d orbitals centered on terminal metals (Cr1 and Cr3), with no contribution from Cr2. For this reason, their energies closely mirror the pattern of LF-split d orbitals of terminal metals, whose coordination environment is only weakly affected by chain length. To achieve an estimate of the zfs in both symmetric and unsymmetric structures at the same level of theory, we followed the quasi-restricted DFT approach devised by Neese et al.[85,87,88] We found that, in spite of the very different extent of unpaired electron delocalization, in both tri- and pentachromium(II) species the D parameter is expected to

be negative and of similar magnitude, with SCN^- axial ligands triggering a slightly higher anisotropy.

In conclusion, the similar S value, magnetic anisotropy, and spin dynamics of tri- and pentachromium(II) EMACs implies by no means a similar pattern of Cr—Cr distances, i.e., the occurrence of a structurally confined Cr^{2+} ion *plus* one or two diamagnetic Cr_2 pairs. In both cases, the d orbitals of terminal ions are invariably the most important contributors to the four SOMOs, at the same time explaining why axial ligands have a small but detectable impact on magnetic anisotropy. However, it should be mentioned that the LF strengths of the axial ligands studied here are quite similar, and therefore, the influence of the axial ligand may be more clearly revealed by comparing complexes with strong (e.g., CN^-) and weak (e.g., BF_4^-) donors. A series of Cr_3 compounds with a variety of axial ligands is currently under examination to confirm the degree of their influence on the magnitude of the relaxation barrier.

■ ASSOCIATED CONTENT

ⓢ Supporting Information

The Supporting Information is available free of charge at https://pubs.acs.org/doi/10.1021/acs.inorgchem.9b02994.

> Additional synthetic procedures, crystallographic and structural tables, details of dc/ac magnetic analyses, EPR diagrams and spectra, additional DFT figures, details of BS-DFT calculation of exchange-coupling constants, and description of the quasi-restricted DFT approach to the D value in tri- and pentachromium(II) EMACs (PDF)
> Input files of BS-DFT calculations on $1a_{sym}$, $1a_{unsym}$, $2a_{sym}$, and $2a_{unsym}$ (PDF)
> Input file of CASSCF calculation on Cr1 in $2a_{unsym}$ (TXT)
> Input file of CASSCF calculation on Cr2—Cr3 in $2a_{unsym}$ (singlet state) (TXT)
> Input file of CASSCF calculation on Cr2—Cr3 in $2a_{unsym}$ (triplet state) (TXT)

Accession Codes

CCDC 1953230 contains the supplementary crystallographic data for this paper. These data can be obtained free of charge via www.ccdc.cam.ac.uk/data_request/cif, or by emailing data_request@ccdc.cam.ac.uk, or by contacting The Cambridge Crystallographic Data Centre, 12 Union Road, Cambridge CB2 1EZ, UK; fax: +44 1223 336033.

■ AUTHOR INFORMATION

Corresponding Authors

Andrea Cornia — *Department of Chemical and Geological Sciences, University of Modena and Reggio Emilia & INSTM, 41125 Modena, Italy;* ⓘ orcid.org/0000-0001-9765-3128; Email: acornia@unimore.it

Elizabeth A. Hillard — *Univ. Bordeaux, CNRS, Centre de Recherche Paul Pascal, CRPP, UMR 5031, 33600 Pessac, France;* Email: elizabeth.hillard@crpp.cnrs.fr

Federico Totti — *Department of Chemistry "Ugo Schiff", University of Florence & INSTM, 50019 Sesto Fiorentino (FI), Italy;* ⓘ orcid.org/0000-0003-4752-0495; Email: federico.totti@unifi.it

Authors

Anne-Laure Barra — *Laboratoire National des Champs Magnétiques Intenses-CNRS, Université Grenoble-Alpes, 38042 Grenoble Cedex 9, France*

Vladimir Bulicanu — *Univ. Bordeaux, CNRS, Centre de Recherche Paul Pascal, CRPP, UMR 5031, 33600 Pessac, France*

Rodolphe Clérac — *Univ. Bordeaux, CNRS, Centre de Recherche Paul Pascal, CRPP, UMR 5031, 33600 Pessac, France;* ⓘ orcid.org/0000-0001-5429-7418

Miguel Cortijo — *Univ. Bordeaux, CNRS, Centre de Recherche Paul Pascal, CRPP, UMR 5031, 33600 Pessac, France*

Rita Galavotti — *Department of Chemical and Geological Sciences, University of Modena and Reggio Emilia & INSTM, 41125 Modena, Italy*

Alessandro Lunghi — *School of Physics and CRANN Institute, Trinity College Dublin, Dublin 2, Ireland;* ⓘ orcid.org/0000-0002-1948-4434

Alessio Nicolini — *Department of Chemical and Geological Sciences, University of Modena and Reggio Emilia & INSTM, 41125 Modena, Italy; Department of Physics, Informatics, and Mathematics, University of Modena and Reggio Emilia, 41125 Modena, Italy*

Mathieu Rouzières — *Univ. Bordeaux, CNRS, Centre de Recherche Paul Pascal, CRPP, UMR 5031, 33600 Pessac, France*

Lorenzo Sorace — *Department of Chemistry "Ugo Schiff", University of Florence & INSTM, 50019 Sesto Fiorentino (FI), Italy;* ⓘ orcid.org/0000-0003-4785-1331

Complete contact information is available at:
https://pubs.acs.org/10.1021/acs.inorgchem.9b02994

Author Contributions

The manuscript was written through contributions of all authors. All authors have given approval to the final version of the manuscript.

Notes

Disclosure: While our manuscript was close to submission, an *ab initio* investigation of **1a** was published by Sakaki et al.[90] They report a similar composition of SOMOs, although their study is unrelated to magnetic anisotropy.

The authors declare no competing financial interest.

■ REFERENCES

(1) Gatteschi, D.; Sessoli, R.; Villain, J. *Molecular Nanomagnets*; Oxford University Press: New York, NY. USA, 2006.

(2) *Molecular Nanomagnets and Related Phenomena*; Gao, S., Ed.; Springer-Verlag: Berlin, Germany, 2015; Structure and Bonding Series 164.

(3) Mannini, M.; Pineider, F.; Danieli, C.; Totti, F.; Sorace, L.; Sainctavit, Ph.; Arrio, M.-A.; Otero, E.; Joly, L.; Cezar, J. C.; Cornia, A.; Sessoli, R. Quantum tunnelling of the magnetization in a

monolayer of oriented single-molecule magnets. *Nature* **2010**, *468* (7322), 417−421.

(4) Malavolti, L.; Lanzilotto, V.; Ninova, S.; Poggini, L.; Cimatti, I.; Cortigiani, B.; Margheriti, L.; Chiappe, D.; Otero, E.; Sainctavit, Ph.; Totti, F.; Cornia, A.; Mannini, M.; Sessoli, R. Magnetic bistability in a submonolayer of sublimated Fe₄ single-molecule magnets. *Nano Lett.* **2015**, *15* (1), 535−541.

(5) Wäckerlin, C.; Donati, F.; Singha, A.; Baltic, R.; Rusponi, S.; Diller, K.; Patthey, F.; Pivetta, M.; Lan, Y.; Klyatskaya, S.; Ruben, M.; Brune, H.; Dreiser, J. Giant Hysteresis of Single-Molecule Magnets Adsorbed on a Nonmagnetic Insulator. *Adv. Mater.* **2016**, *28* (26), 5195−5199.

(6) Katoh, K.; Komeda, T.; Yamashita, M. The Frontier of Molecular Spintronics Based on Multiple-Decker Phthalocyaninato TbᴵᴵᴵSingle-Molecule Magnets. *Chem. Rec.* **2016**, *16* (2), 987−1016.

(7) Moreno-Pineda, E.; Godfrin, C.; Balestro, F.; Wernsdorfer, W.; Ruben, M. Molecular spin qudits for quantum algorithms. *Chem. Soc. Rev.* **2018**, *47* (2), 501−513.

(8) Cornia, A.; Seneor, P. Spintronics: The molecular way. *Nat. Mater.* **2017**, *16* (5), 505−506.

(9) Gaita-Ariño, A.; Luis, F.; Hill, S.; Coronado, E. Molecular spins for quantum computation. *Nat. Chem.* **2019**, *11* (4), 301−309.

(10) Gómez-Coca, S.; Aravena, D.; Morales, R.; Ruiz, E. Large magnetic anisotropy in mononuclear metal complexes. *Coord. Chem. Rev.* **2015**, *289−290*, 379−392.

(11) Atanasov, M.; Aravena, D.; Suturina, E.; Bill, E.; Maganas, D.; Neese, F. First principles approach to the electronic structure, magnetic anisotropy and spin relaxation in mononuclear 3d-transition metal single molecule magnets. *Coord. Chem. Rev.* **2015**, *289−290*, 177−214.

(12) Gómez-Coca, S.; Urtizberea, A.; Cremades, E.; Alonso, P. J.; Camón, A.; Ruiz, E.; Luis, F. Origin of slow magnetic relaxation in Kramers ions with non-uniaxial anisotropy. *Nat. Commun.* **2014**, *5* (1), 4300.

(13) Feng, M.; Tong, M.-L. Single Ion Magnets from 3d to 5f: Developments and Strategies. *Chem. - Eur. J.* **2018**, *24* (30), 7574−7594.

(14) Lunghi, A.; Totti, F.; Sessoli, R.; Sanvito, S. The role of anharmonic phonons in under-barrier spin relaxation of single molecule magnets. *Nat. Commun.* **2017**, *8*, 14620.

(15) Escalera-Moreno, L.; Baldoví, J. J.; Gaita-Ariño, A.; Coronado, E. Spin states, vibrations and spin relaxation in molecular nano-magnets and spin qubits: a critical perspective. *Chem. Sci.* **2018**, *9* (13), 3265−3275.

(16) Bunting, P. C.; Atanasov, M.; Damgaard-Møller, E.; Perfetti, M.; Crassee, I.; Orlita, M.; Overgaard, J.; van Slageren, J.; Neese, F.; Long, J. R. A linear cobalt(II) complex with maximal orbital angular momentum from a non-Aufbau ground state. *Science (Washington, DC, U. S.)* **2018**, *362* (6421), eaat7319.

(17) Bar, A. K.; Kalita, P.; Singh, M. K.; Rajaraman, G.; Chandrasekhar, V. Low-coordinate mononuclear lanthanide complexes as molecular nanomagnets. *Coord. Chem. Rev.* **2018**, *367*, 163−216.

(18) Gupta, S. K.; Murugavel, R. Enriching lanthanide single-ion magnetism through symmetry and axiality. *Chem. Commun.* **2018**, *54* (30), 3685−3696.

(19) Liu, J.-L.; Chen, Y.-C.; Tong, M.-L. Symmetry strategies for high performance lanthanide-based single-molecule magnets. *Chem. Soc. Rev.* **2018**, *47* (7), 2431−2453.

(20) Ding, Y.-S.; Chilton, N. F.; Winpenny, R. E. P.; Zheng, Y.-Z. On Approaching the Limit of Molecular Magnetic Anisotropy: A Near-Perfect Pentagonal Bipyramidal Dysprosium(III) Single-Molecule Magnet. *Angew. Chem., Int. Ed.* **2016**, *55* (52), 16071−16074.

(21) Chilton, N. F. Design criteria for high-temperature single-molecule magnets. *Inorg. Chem.* **2015**, *54* (5), 2097−2099.

(22) Guo, F.-S.; Day, B. M.; Chen, Y.-C.; Tong, M.-L.; Mansikkamäki, A.; Layfield, R. A. A Dysprosium Metallocene Single-Molecule Magnet Functioning at the Axial Limit. *Angew. Chem., Int. Ed.* **2017**, *56* (38), 11445−11449.

(23) Goodwin, C. A. P.; Ortu, F.; Reta, D.; Chilton, N. F.; Mills, D. P. Molecular magnetic hysteresis at 60 kelvin in dysprosocenium. *Nature* **2017**, *548* (7668), 439−442.

(24) Guo, F.-S.; Day, B. M.; Chen, Y.-C.; Tong, M.-L.; Mansikkamäki, A.; Layfield, R. A. Magnetic hysteresis up to 80 kelvin in a dysprosium metallocene single-molecule magnet. *Science (Washington, DC, U. S.)* **2018**, *362* (6421), 1400−1403.

(25) Hernández Sánchez, R.; Betley, T. A. Thermally Persistent High-Spin Ground States in Octahedral Iron Clusters. *J. Am. Chem. Soc.* **2018**, *140* (48), 16792−16806.

(26) Majumdar, M.; Bera, J. K. Transition-Metal-Based Linear Chain Compounds. In *Macromolecules Containing Metal and Metal-like Elements, Vol. 9: Supramolecular and Self-Assembled Metal-Containing Materials*; Abd-El Aziz, A. S., Carraher, C. E., Pittman, C. U., Zeldin, M., Eds.; John Wiley & Sons, Inc.: Hoboken, NJ, 2009; Chapter 5, pp 181−253.

(27) Berry, J. F. Metal−Metal Bonds in Chains of Three or More Metal Atoms: From Homometallic to Heterometallic Chains. *Struct. Bonding (Berlin, Ger.)* **2010**, *136*, 1−28.

(28) Hua, S.-A.; Cheng, M.-C.; Chen, C.; Peng, S.-M. From Homonuclear Metal String Complexes to Heteronuclear Metal String Complexes. *Eur. J. Inorg. Chem.* **2015**, *2015* (15), 2510−2523.

(29) Chen, P.-J.; Sigrist, M.; Horng, E.-C.; Lin, G.-M.; Lee, G.-H.; Chen, C.; Peng, S.-M. A ligand design with a modified naphthyridylamide for achieving the longest EMACs: the 1st single-molecule conductance of an undeca-nickel metal string. *Chem. Commun.* **2017**, *53* (34), 4673−4676.

(30) Srinivasan, A.; Cortijo, M.; Bulicanu, V.; Naim, A.; Clérac, R.; Sainctavit, Ph.; Rogalev, A.; Wilhelm, F.; Rosa, P.; Hillard, E. A. Enantiomeric resolution and X-ray optical activity of a tricobalt extended metal atom chain. *Chem. Sci.* **2018**, *9* (5), 1136−1143.

(31) Yu, C.-H.; Kuo, M.-S.; Chuang, C.-Y.; Lee, G.-H.; Hua, S.-A.; Jin, B.-Y.; Peng, S.-M. Chirality Control of Quadruple Helixes of Metal Strings by Peripheral Chiral Ligands. *Chem. - Asian J.* **2014**, *9* (11), 3111−3115.

(32) Nicolini, A.; Galavotti, R.; Barra, A.-L.; Borsari, M.; Caleffi, M.; Luo, G.; Novitchi, G.; Park, K.; Ranieri, A.; Rigamonti, L.; Roncaglia, F.; Train, C.; Cornia, A. Filling the Gap in Extended Metal Atom Chains: Ferromagnetic Interactions in a Tetrairon(II) String Supported by Oligo-α-pyridylamido Ligands. *Inorg. Chem.* **2018**, *57* (9), 5438−5448.

(33) Clérac, R.; Cotton, F. A.; Daniels, L. M.; Dunbar, K. R.; Murillo, C. A.; Pascual, I. Linear Trichromium Complexes with Direct Cr to Cr Contacts. 1. Compounds with Cr₃(dipyridylamide)₄²⁺ Cores. *Inorg. Chem.* **2000**, *39* (4), 748−751.

(34) Chang, H.-C.; Li, J.-T.; Wang, C.-C.; Lin, T.-W.; Lee, H.-C.; Lee, G.-H.; Peng, S.-M. Linear Five-Centred Chromium Multiple Bonds Bridged by Four tpda²⁻ Ligands [tpda²⁻ = tripyridyldiamido dianion] − Synthesis and Structural Studies. *Eur. J. Inorg. Chem.* **1999**, *1999* (8), 1243−1251.

(35) Cornia, A.; Rigamonti, L.; Boccedi, S.; Clérac, R.; Rouzières, M.; Sorace, L. Magnetic blocking in extended metal atom chains: A pentachromium(II) complex behaving as a single-molecule magnet. *Chem. Commun.* **2014**, *50* (96), 15191−15194.

(36) Christian, J. H.; Brogden, D. W.; Bindra, J. K.; Kinyon, J. S.; van Tol, J.; Wang, J.; Berry, J. F.; Dalal, N. S. Enhancing the Magnetic Anisotropy of Linear Cr(II) Chain Compounds Using Heavy Metal Substitutions. *Inorg. Chem.* **2016**, *55* (13), 6376−6383.

(37) Wang, J.; Wang, Z.; Clark, R. J.; Ozarowski, A.; van Tol, J.; Dalal, N. S. A high-frequency EPR characterization of the S = 2 linear tri-atomic chain in Cr₃(dpa)₄Cl₂·CH₂Cl₂. *Polyhedron* **2011**, *30* (18), 3058−3061.

(38) Berry, J. F.; Cotton, F. A.; Fewox, C. S.; Lu, T.; Murillo, C. A.; Wang, X. Extended metal atom chains (EMACs) of five chromium or cobalt atoms: Symmetrical or unsymmetrical? *Dalton Trans.* **2004**, No. 15, 2297−2302.

(39) Dirvanauskas, A.; Galavotti, R.; Lunghi, A.; Nicolini, A.; Roncaglia, F.; Totti, F.; Cornia, A. Solution structure of a pentachromium(II) single molecule magnet from DFT calculations,

isotopic labelling and multinuclear NMR spectroscopy. *Dalton Trans.* **2018**, *47* (2), 585−595.

(40) Wang, W.-Z.; Ismayilov, R. H.; Lee, G.-H.; Huang, Y.-L.; Yeh, C.-Y.; Fu, M.-D.; Chen, C.; Peng, S.-M. Fine tuning of pentachromium(II) metal string complexes through elaborate design of ligand. *New J. Chem.* **2012**, *36* (3), 632−637.

(41) Ismayilov, R. H.; Wang, W.-Z.; Lee, G.-H.; Chien, C.-H.; Jiang, C.-H.; Chiu, C.-L.; Yeh, C.-Y.; Peng, S.-M. Redox Modification of EMACs Through the Tuning of Ligands: Heptametal(II) Complexes of Pyrazine-Modulated Oligo-α-pyridylamido Ligands. *Eur. J. Inorg. Chem.* **2009**, *2009* (14), 2110−2120.

(42) Ismayilov, R. H.; Wang, W.-Z.; Wang, R.-R.; Yeh, C.-Y.; Lee, G.-H.; Peng, S.-M. Four quadruple metal−metal bonds lined up: linear nonachromium(II) metal string complexes. *Chem. Commun.* **2007**, No. 11, 1121−1123.

(43) Berry, J. F.; Cotton, F. A.; Lu, T.; Murillo, C. A.; Roberts, B. K.; Wang, X. Molecular and electronic structures by design: Tuning symmetrical and unsymmetrical linear trichromium chains. *J. Am. Chem. Soc.* **2004**, *126* (22), 7082−7096.

(44) Berry, J. F.; Cotton, F. A.; Murillo, C. A.; Roberts, B. K. An Efficient Synthesis of Acetylide/Trimetal/Acetylide Molecular Wires. *Inorg. Chem.* **2004**, *43* (7), 2277−2283.

(45) Ismayilov, R. H.; Wang, W.-Z.; Lee, G.-H.; Wang, R.-R.; Liu, I. P.-C.; Yeh, C.-Y.; Peng, S.-M. New versatile ligand family, pyrazine-modulated oligo-α-pyridylamino ligands, from coordination polymer to extended metal atom chains. *Dalton Trans.* **2007**, No. 27, 2898−2907.

(46) Wu, L.-C.; Thomsen, M. K.; Madsen, S. R.; Schmoekel, M.; Jørgensen, M. R. V.; Cheng, M.-C.; Peng, S.-M.; Chen, Y.-S.; Overgaard, J.; Iversen, B. B. Chemical Bonding in a Linear Chromium Metal String Complex. *Inorg. Chem.* **2014**, *53* (23), 12489−12498.

(47) Benbellat, N.; Rohmer, M.-M.; Bénard, M. Electronic origin of the structural versatility in linear trichromium complexes of dipyridylamide *Chem. Commun.* **2001**, No. 22, 2368−2369

(48) Georgiev, V. P.; McGrady, J. E. Influence of Low-Symmetry Distortions on Electron Transport through Metal Atom Chains: When Is a Molecular Wire Really "Broken"? *J. Am. Chem. Soc.* **2011**, *133* (32), 12590−12599.

(49) Georgiev, V. P.; Mohan, P. J.; DeBrincat, D.; McGrady, J. E. Low-symmetry distortions in Extended Metal Atom Chains (EMACs): Origins and consequences for electron transport. *Coord. Chem. Rev.* **2013**, *257* (1), 290−298.

(50) Spivak, M.; Arcisauskaite, V.; López, X.; McGrady, J. E.; de Graaf, C. A multiconfigurational approach to the electronic structure of trichromium extended metal atom chains. *Dalton Trans.* **2017**, *46* (19), 6202−6211.

(51) Spivak, M.; Arcisauskaite, V.; López, X.; de Graaf, C. Backbone flexibility of extended metal atom chains. Ab initio molecular dynamics for $Cr_3(dpa)_4X_2$ (X = NCS, CN, NO_3) in gas and crystalline phases. *Dalton Trans.* **2017**, *46* (44), 15487−15493.

(52) Berry, J. F.; Cotton, F. A.; Murillo, C. A.; Chan, Z.-K.; Yeh, C.-W.; Chen, J.-D. Linear Trichromium, Tricobalt, Trinickel, and Tricopper Complexes of 2,2′-Dipyridylamine. *Inorg. Syn.* **2014**, *36*, 103−110.

(53) Turov, Y.; Berry, J. F. Synthesis, characterization and thermal properties of trimetallic N_3−Cr≡Cr⋯M−N_3 azide complexes with M = Cr, Mn, Fe, and Co. *Dalton Trans.* **2012**, *41* (26), 8153−8161.

(54) *APEX2, SADABS, and SAINT Software Reference Manuals*; Bruker-AXS, Inc.: Madison, WI, USA, 2009.

(55) Sheldrick, G. M. Crystal structure refinement with *SHELXL*. *Acta Crystallogr., Sect. C: Struct. Chem.* **2015**, *71* (1), 3−8.

(56) Bain, G. A.; Berry, J. F. Diamagnetic Corrections and Pascal's Constants. *J. Chem. Educ.* **2008**, *85* (4), 532−536.

(57) Cole, K. S.; Cole, R. H. Dispersion and Absorption in Dielectrics I. Alternating Current Characteristics. *J. Chem. Phys.* **1941**, *9* (4), 341−351.

(58) Dekker, C.; Arts, A. F. M.; de Wijn, H. W.; van Duyneveldt, A. J.; Mydosh, J. A. Activated dynamics in a two-dimensional Ising spin glass: $Rb_2Cu_{1−x}Co_xF_4$. *Phys. Rev. B: Condens. Matter Mater. Phys.* **1989**, *40* (16), 11243−11251.

(59) Mossin, S.; Weihe, H.; Barra, A.-L. Is the Axial Zero-Field Splitting Parameter of Tetragonally Elongated High-Spin Manganese-(III) Complexes Always Negative? *J. Am. Chem. Soc.* **2002**, *124* (30), 8764−8765.

(60) Jacobsen, C. J. H.; Pedersen, E.; Villadsen, J.; Weihe, H. ESR characterization of *trans*-$V^{II}(py)_4X_2$ and *trans*-$Mn^{II}(py)_4X_2$ (X = NCS, Cl, Br, I; py = pyridine). *Inorg. Chem.* **1993**, *32* (7), 1216−1221.

(61) Bencini, A.; Ciofini, I.; Uytterhoeven, M. G. Angular overlap calculations of the spin Hamiltonian parameters of transition metal ions in low symmetry environments. High spin iron(II), iron(III) and manganese(III). *Inorg. Chim. Acta* **1998**, *274* (1), 90−101.

(62) Lever, A. B. P. *Inorganic Electronic Spectroscopy*, 2nd ed.; Elsevier: Amsterdam, The Netherlands, 1984.

(63) Bencini, A.; Benelli, C.; Gatteschi, D. The angular overlap model for the description of the paramagnetic properties of transition metal complexes. *Coord. Chem. Rev.* **1984**, *60*, 131−169.

(64) Khamar, M. M.; Larkworthy, L. F.; Nelson-Richardson, M. H. O. Complexes of chromium(II) halides with methylpyridines. *Inorg. Chim. Acta* **1978**, *28*, 245−250.

(65) Neese, F. The *ORCA* program system. *Wiley Interdiscip. Rev.: Comput. Mol. Sci.* **2012**, *2* (1), 73−78.

(66) Segall, M. D.; Shah, R.; Pickard, C. J.; Payne, M. C. Population analysis of plane-wave electronic structure calculations of bulk materials. *Phys. Rev. B: Condens. Matter Mater. Phys.* **1996**, *54* (23), 16317−16320.

(67) Grimme, S.; Antony, J.; Ehrlich, S.; Krieg, H. A consistent and accurate ab initio parametrization of density functional dispersion correction (DFT-D) for the 94 elements H-Pu. *J. Chem. Phys.* **2010**, *132* (15), 154104.

(68) Pantazis, D. A.; Chen, X.-Y.; Landis, C. R.; Neese, F. All-Electron Scalar Relativistic Basis Sets for Third-Row Transition Metal Atoms. *J. Chem. Theory Comput.* **2008**, *4* (6), 908−919.

(69) Weigend, F.; Ahlrichs, R. Balanced basis sets of split valence, triple zeta valence and quadruple zeta valence quality for H to Rn: Design and assessment of accuracy. *Phys. Chem. Chem. Phys.* **2005**, *7* (18), 3297−3305.

(70) Lin, S.-Y.; Chen, I.-W. P.; Chen, C.; Hsieh, M.-H.; Yeh, C.-Y.; Lin, T.-W.; Chen, Y.-H.; Peng, S.-M. Effect of Metal−Metal Interactions on Electron Transfer: an STM Study of One-Dimensional Metal String Complexes. *J. Phys. Chem. B* **2004**, *108* (3), 959−964.

(71) Llunell, M.; Casanova, D.; Cirera, J.; Alemany, P.; Alvarez, S. *SHAPE*, version 2.1, Continuous Shape Measures calculation; Universitat de Barcelona: Spain, 2013.

(72) Stoll, S.; Schweiger, A. *EasySpin*, a comprehensive software package for spectral simulation and analysis in EPR. *J. Magn. Reson.* **2006**, *178* (1), 42−55.

(73) Reta, D.; Chilton, N. F. Uncertainty estimates for magnetic relaxation times and magnetic relaxation parameters. *Phys. Chem. Chem. Phys.* **2019**, *21* (42), 23567−23575.

(74) Deng, Y.-F.; Han, T.; Wang, Z.; Ouyang, Z.; Yin, B.; Zheng, Z.; Krzystek, J.; Zheng, Y.-Z. Uniaxial magnetic anisotropy of square-planar chromium(II) complexes revealed by magnetic and HF-EPR studies. *Chem. Commun.* **2015**, *51* (100), 17688−17691.

(75) Gatteschi, D.; Sorace, L.; Sessoli, R.; Barra, A.-L. High-frequency EPR: An occasion for revisiting ligand field theory. *Appl. Magn. Reson.* **2001**, *21* (3−4), 299−310.

(76) Krzystek, J.; Telser, J.; Pardi, L. A.; Goldberg, D. P.; Hoffman, B. M.; Brunel, L.-C. High-Frequency and -Field Electron Paramagnetic Resonance of High-Spin Manganese(III) in Porphyrinic Complexes. *Inorg. Chem.* **1999**, *38* (26), 6121−6129.

(77) Telser, J.; Pardi, L. A.; Krzystek, J.; Brunel, L.-C. EPR Spectra from "EPR-Silent" Species: High-Field EPR Spectroscopy of Aqueous Chromium(II). *Inorg. Chem.* **2000**, *39* (8), 1834−1834.

(78) Barra, A.-L.; Gatteschi, D.; Sessoli, R.; Abbati, G. L.; Cornia, A.; Fabretti, A. C.; Uytterhoeven, M. G. Electronic structure of

manganese(III) compounds from high-frequency EPR spectra. *Angew. Chem., Int. Ed. Engl.* **1997**, *36* (21), 2329−2331.

(79) Telser, J. A perspective on applications of ligand-field analysis: inspiration from electron paramagnetic resonance spectroscopy of coordination complexes of transition metal ions. *J. Braz. Chem. Soc.* **2006**, *17* (8), 1501−1515.

(80) Bencini, A.; Gatteschi, D. *Electron Paramagnetic Resonance of Exchange Coupled Systems*; Springer-Verlag: Berlin, Germany, 1990.

(81) Cotton, F. A.; Daniels, L. M.; Murillo, C. A.; Wang, X. Getting the right answer to a key question concerning molecular wires *Chem. Commun.* No. 24, 2461−2462

(82) Cotton, F. A. Chromium Compounds. In *Multiple Bonds between Metal Atoms*; Cotton, F. A., Murillo, C. A., Walton, R. A., Eds.; Springer Science and Business Media: New York, NY, USA, 2005; Chapter 3, pp 35−68.

(83) Bencini, A.; Totti, F. A Few Comments on the Application of Density Functional Theory to the Calculation of the Magnetic Structure of Oligo-Nuclear Transition Metal Clusters. *J. Chem. Theory Comput.* **2009**, *5* (1), 144−154.

(84) Bencini, A.; Totti, F. DFT description of the magnetic structure of polynuclear transition-metal clusters: The complexes [{Cu-(bpca)$_2$(H$_2$O)$_2$}{Cu(NO$_3$)$_2$}$_2$], (bpca = Bis(2-pyridylcarbonyl)-amine), and [Cu(DBSQ)(C$_2$H$_5$O)]$_2$, (DBSQ = 3,5-di-*tert*-butyl-semiquinonato). *Int. J. Quantum Chem.* **2005**, *101* (6), 819−825.

(85) Neese, F. Calculation of the zero-field splitting tensor on the basis of hybrid density functional and Hartree-Fock theory. *J. Chem. Phys.* **2007**, *127* (16), 164112.

(86) Cotton, F. A.; Felthouse, T. R. Pyridine and pyrazine adducts of tetrakis(acetato)dichromium. *Inorg. Chem.* **1980**, *19* (2), 328−331.

(87) Neese, F.; Solomon, E. I. Calculation of Zero-Field Splittings, g-Values, and the Relativistic Nephelauxetic Effect in Transition Metal Complexes. Application to High-Spin Ferric Complexes. *Inorg. Chem.* **1998**, *37* (26), 6568−6582.

(88) Neese, F. Importance of Direct Spin−Spin Coupling and Spin-Flip Excitations for the Zero-Field Splittings of Transition Metal Complexes: A Case Study. *J. Am. Chem. Soc.* **2006**, *128* (31), 10213−10222.

(89) Liakos, D. G.; Ganyushin, D.; Neese, F. A Multiconfigurational ab Initio Study of the Zero-Field Splitting in the Di- and Trivalent Hexaquo−Chromium Complexes. *Inorg. Chem.* **2009**, *48* (22), 10572−10580.

(90) Nakagaki, M.; Nakatani, N.; Sakaki, S. How to understand very weak Cr−Cr double bonds and negative spin populations in trinuclear Cr complexes: theoretical insight. *Phys. Chem. Chem. Phys.* **2019**, *21* (41), 22976−22989.

■ NOTE ADDED AFTER ASAP PUBLICATION

This paper was published ASAP on January 22, 2020, with errors in eqs 2 and 3 and the title of Table 3 and small errors in the text and references. The corrected version was posted on January 23, 2020.